RSC Advances

ROYAL SOCIETY OF CHEMISTRY

www.rsc.org/advances

Advanced Chemical Compositions and Nanoarchitectures of Bismuth Based Complex Oxides for Solar Photocatalytic Application

Songmei Sun and Wenzhong Wang*

State Key Laboratory of High Performance Ceramics and Superfine Microstructure, Shanghai Institute of Ceramics, Chinese Academy of Sciences

1295 Dingxi Road, Shanghai 200050, P. R. China

Abstract: Bismuth based complex oxides have attracted considerable interest due to their great potential to harvest solar light to solve the current environmental and energy crisis. Bismuth based complex oxides have excellent photo-oxidation ability for organic contaminant degradation and water oxidation via a photocatalytic process. Many efforts have been made to improve their photocatalytic performance, especially on the $BiVO_4$, Bi_2WO_6 and Bi_2MoO_6 materials, which have been mostly studied in the past few years. Significant progress in understanding the fundamentals and improving the photocatalytic performance has been made due to the various new developed concepts and approaches in recent years. In this review, we present a comprehensive overview on the fundamentals and recent advances of $BiVO_4$, Bi_2WO_6 and Bi_2MoO_6 photocatalysts. After the analysis of the structure-property relationships, the strategies that have been employed to enhance their photocatalytic performance are discussed in detail, including morphology control, surface modification, doping and construction of composite material. Furthermore, remarks on the challenges and perspectives of research directions are proposed for further development of the highly efficient bismuth based complex oxide photocatalysts.

Keywords: bismuth based photocatalyst; structure-property relationships; effective photocatalyst design; water purification

* Corresponding author, Fax: +86-21-5241-3122, Email: wzwang@mail.sic.ac.cn

Photographs and brief biographies for authors

Songmei Sun

Songmei Sun received her BSc degree in Material Science and Engineering in 2005 at Shandong University of Technology and Ph.D. degree in Material Physics and Chemistry in 2010 from Shanghai Institute of Ceramics, Chinese Academy of Sciences. She has published more than 50 papers in the area of bismuth based oxide photocatalyst up to the present. She is currently an associate professor in Shanghai Institute of Ceramics, Chinese Academy of Sciences. Her current research is focused on the rational synthesis and mechanism exploration of bismuth based complex oxides for solar light driven photocatalysis.

Wenzhong Wang

Wenzhong Wang received his Ph.D. degree from University of Science and Technology of China in 1998. He worked as a postdoctoral fellow at Virginia Commonwealth University, Rutgers University and Colorado State University from 1999 to 2003. In 2004, he was supported by “Hundred Talents Program”, CAS. He currently is a full professor in Shanghai Institute of Ceramics, Chinese Academy of

Sciences. His research interests include controlled fabrication, novel properties and photocatalytic applications of semiconductor nanostructures, especially with a focus on bismuth based semiconductors for environmental purification and solar light conversion.

1 General Background

With the rapid development of industry, environmental pollution and energy crisis have been serious challenges for human beings. Photocatalysis, which could harvest energy directly from sunlight, offers a desirable approach to solving these two problems. Over the past few decades, photocatalysis has been widely investigated both theoretically and technologically after the Honda–Fujishima effect of water splitting using TiO_2 electrode was reported in the early 1970s.[1-7] However, the typical photocatalyst TiO_2 is only active in the ultraviolet (UV) light range. Its wide band gap limits its practical applications under solar light. Although modification of TiO_2 by doping has been used to increase the visible light absorption,[8-11] doped materials often suffer from thermal instability and some dopants may function as recombination centers to decrease the photocatalytic performance.[8]

With this recognition, many recent studies have been focused on the development of non-TiO_2 based semiconductors that can serve as efficient solar light driven photocatalysts. Topics covered the chemical compositions, synthetic strategies, and structure-property relationships etc. Desirable photocatalysts should have a small band gap to increase the solar energy utilization efficiency and appropriate band edge positions to facilitate the light induced redox reactions. In other words, the valence band edge of an ideal photocatalyst is expected positive enough to provide sufficient overpotential for photo-oxidation reaction and the conduction band edge is negative enough for photo-reduction reaction. In the last several years, numerous studies on the visible light driven photocatalyst have proved it is difficult to find a stable semiconductor satisfying both cases. One viable option is the development of narrow band semiconductor with high photo-oxidation activity, for the light induced contaminant degradation and water oxidation mainly depend on the photo-oxidation

ability of a photocatalyst. Noticeably, the major challenge for water splitting is the water oxidation process, which is an uphill reaction involved four-electron transfer with slow kinetics. Therefore, metal oxide semiconductors with intrinsic narrow band gap and deep valence bands attracted more and more attention on the development of visible light driven photocatalyst.[12-19] Although the deep valence bands endow these oxide photocatalyst high photo-oxidation ability, the photocatalytic efficiency is usually low because the excessive recombination of the photogenerated charge carriers. In the process of searching for efficient visible light driven oxide photocatalyst, bismuth based complex oxides were recognized as potential candidates. It was suggested the lone-pair distortion of Bi 6s orbital in these semiconductors may cause the pronounced overlap of O 2p and Bi 6s orbitals in the valence band, which is benefit to the mobility of photogenerated charge carriers for improving the photocatalytic activity.[20-24] Consequently, a great deal of effort was then devoted to the development of bismuth based complex oxide photocatalysts, such as $BiVO_4$,[25-31] Bi_2WO_6,[32-36] Bi_2MoO_6,[37-39] $Bi_4Ti_3O_{12}$,[40-42] $BiFeO_3$,[43-48] $Bi_2Fe_4O_9$,[49-52] $Bi_5FeTi_3O_{15}$,[53] BiOCl,[54-56] Bi_5O_7I[57,58] et al. Compared with their simple oxides without bismuth atoms, these complex oxides exhibited excellent photocatalytic activity by virtue of the improved charge transfer. However, the typical efficiencies of these bismuth based complex oxides were not satisfying because of their low conduction band levels and insufficient visible light absorption. There is still a great deal of effort to do for further improving their photocatalytic performance.

The critical process for semiconductor photocatalysis is the generation of electron-hole pairs, followed by the separation and transfer of the electrons and holes. Therefore, there are mainly two general approaches to improve the photocatalytic performance of bismuth based complex oxides. One way is to enhance the light

absorption. Another way is to improve the utilization efficiency of the photo-generated carries, such as by decreasing the recombination rate and increasing the life time of the photo-generated carries. In the previous studies on the bismuth based complex oxide photocatalysts, it was found all of these processes are seriously affected by the composition and structure of the photocatalyst. Various strategies such as morphology control, doping, and construction of composite material, have been developed recently to improve their photocatalytic performance. Some basic principles of photocatalysis in bismuth based complex oxides may be concluded by systematically studying the obtained results up to the present. For this, Zhang et al.[59] and Zhu et al.[60] independently summarized a short review of Bi_2WO_6 photocatalyst on the controllable synthesis, microstructures and environmental application, mainly based on their contribution to this area. Choi et al. reviewed the $BiVO_4$ photoanodes for use in photoelectrochemical (PEC) water oxidation,[61] but the studies on the suspension-type $BiVO_4$ used as photocatalysts for water oxidation or pollutant degradation were not included. Considering the great potential of bismuth based complex oxides, a systematic study on these materials is necessary to find out the fundamental principles for the construction of high-performance, commercial available solar light photocatalytic material.

Herein, we provide a comprehensive review of bismuth based complex oxides photocatalysts by focusing on the mostly studied $BiVO_4$, Bi_2WO_6 and Bi_2MoO_6 materials. It is the first complex work on bismuth based complex oxides covering the primary important factors for photocatalysis. In this review, the bases of bismuth based complex oxides will be first discussed, including the crystal structure, the electronic structure and the structure-performance relationship. Then the major factors affecting photocatalytic performances and strategies to improving the photocatalytic

activity will be critically reviewed. For each section, we provide critical commentary based on our knowledge and related research experiences. This review contains the latest ideas and concepts in understanding the basis and improving the performance of bismuth based complex oxide photocatalyst. Representative works were selected from the most recent literature available. The intent of this review is to give the readers a critical discussion of the progress and perspective of bismuth based complex oxide photocatalysts, which could provide guidance for the designed synthesis of high-performance solar light driven photocatalyst.

2. Bases of Bi-M-O complex oxide (M=V, W, Mo) photocatalysts

Photocatalytic activity is closely related to the crystal and electronic structures. In this section, we present an overview on the crystal and electronic structures of Bi-M-O complex oxides and discuss how they affect its photocatalytic performance. This is indispensible for developing effective strategies to obtain highly efficient photocatalysts.

2.1 Crystal structure

$BiVO_4$ is known to exist in three crystalline phases: tetragonal zircon, monoclinic scheelite, and tetragonal scheelite structure.[62] The process of phase transformation among them has been studied. When tetragonal zircon $BiVO_4$ is heat-treated above 670-770 K, monoclinic scheelite $BiVO_4$ was obtained. Among scheelite structures, the tetragonal phase is a high temperature phase and the phase transition between monoclinic scheelite $BiVO_4$ and tetragonal scheelite $BiVO_4$ was observed to occur reversibly at 528 K.[63] The tetragonal zircon $BiVO_4$ has a band gap of 2.9 eV. Its photocataytic activity was low under visible light irradiation.[20] Therefore, the mostly studied $BiVO_4$ photocatalysts at present is the scheelite BiVO4 with a band gap of 2.4

eV. Fig. 1a shows the crystal structure of scheelite $BiVO_4$ along the [100] direction. It was found a layered structure of Bi-V-O units stacked parallel to the c axis. In this structure, each V ion is coordinated by four oxygen atoms forming a VO_4 tetrahedron. Each VO_4 tetrahedron does not make contact with a subsequent VO_4 tetrahedron, and each Bi ion is coordinated by eight oxygen atoms from eight different VO_4 tetrahedrons.[64]

There are two types of O atom in this structure. O1 is coordinated to one Bi and V, while O2 is coordinated to two Bi and a single V. The only difference between the tetragonal and monoclinic scheelite structure is that the local environments of V and Bi ions are more significantly distorted in the monoclinic structure, which removes the four-fold symmetry necessary for a tetragonal system. For example, the lengths of the four V–O bond (1.72 Å) were equal in tetragonal scheelite, but two different V–O bond lengths exist in a monoclinic scheelite structure (1.77 Å and 1.69 Å). In the same manner, while only two very similar Bi–O distances exist in the tetragonal scheelite structure (2.453 Å and 2.499 Å), there are four different Bi–O distances (2.354 Å, 2.372 Å, 2.516 Å and 2.628 Å) in the monoclinic scheelite structure.[61,64] The band gap of $BiVO_4$ (s-m) (2.41 eV) was similar to that of $BiVO_4$ (s -t) (2.34 eV), suggesting the energy structures were similar to each other.[65] However, $BiVO_4$ (s-m) showed high activity. The disparate photocatalytic activity is originated from the variations of the crystal structure, which result in the modification of the electronic structure. Akihiko and co-workers considered that the distortion of a Bi-O polyhedron by a $6s^2$ lone pair of Bi^{3+} play an important role in improving the photocatalytic performance of monoclinic $BiVO_4$ under visible light irradiation.[65] The further distortion of the Bi-polyhedra in the monoclinic scheelite structure endows its higher activity than tetragonal scheelite structure. These indicate that the photocatalytic

performance of $BiVO_4$ largely depends on the crystal structure.

Different from $BiVO_4$, there are only two crystalline phases in Bi_2MO_6 (M = Mo, W) compounds: orthorhombic and monoclinic structure. Orthorhombic structures of Bi_2MO_6 (M = Mo, W) existed at low and intermediate temperatures (T < 960 ℃) and monoclinic structure is a high temperature phase (T > 960 ℃).[66,67] The presently studied Bi_2MO_6 (M = Mo, W) photocatalyst was usually orthorhombic phase. Fig. 1b and c show the schematic crystal structure of the orthorhombic Bi_2WO_6 and Bi_2MoO_6, respectively. It is obvious the Bi_2MO_6 (M=Mo, W) photocatalysts possess a layered structure which is composed of MO_6 octahedral layers and Bi–O–Bi layers. In this structure, each Bi atom is coordinated with four O and four M atoms. Each M atom is coordinated with six O atoms to form MO_6 octahedron. The MO_6 octahedrons are connected to each other by corner-sharing O atom. The $(Bi_2O_2)^{2+}$ layers are sandwiched between MO_6 octahedral layers. The local environments of M and Bi ions are also distorted in the orthorhombic Bi_2MO_6 (M=Mo, W). For low temperature orthorhombic Bi_2WO_6 as an example, there are six different W–O bond lengths (1.85 Å, 1.87 Å, 1.728 Å, 1.720 Å, 2.240 Å and 2.215 Å) exist in the WO_6 octahedron.[67] indicating a distorted octahedral structure. The off-centre octahedral distortions are a general feature of the structural chemistry of d^0 metal cations. It also existed in the orthorhombic Bi_2MoO_6 photocatalyst.

Based on the above analysis, it was found both of the $BiVO_4$ and Bi_2MO_6 (M = Mo, W) photocatalysts possess a layer structure with local lattice distortions. Besides the reasons mentioned above for the crystal distortion, it is worth noting that the Bi 6s lone pair electrons is another driving force for asymmetric coordination environments in the Bi-M-O photocatalyst. The distortion of local crystal structure probably affects the electronic structure, which is responsible for the high visible light photocatalytic

activity.

2.2 Electronic structure

The schematic band structure of the Bi-M-O compounds was shown in Fig. 2. All of the $BiVO_4$ and Bi_2MO_6 (M=Mo, W) photocatalysts have a direct band gap. Density functional theory (DFT) calculations by many researchers have show that the valence band of the $BiVO_4$ and Bi_2MO_6 (M=Mo, W) photocatalysts was mainly composed of O 2p and Bi 6s levels, while the conduction band was mainly composed of M nd (V 3d, Mo 4d, W 5d) levels.[23, 68-71]The band structure indicates that charge transfer upon photoexcitation occurs from the O 2p + Bi 6s hybrid orbitals to the empty M nd orbitals. These authors also emphasized the importance of the sterically active Bi $6s^2$ lone pair for both reducing the oxide band gaps and increasing the hole conductivity,[69] for the Bi 6s orbits are located upon the O 2p orbits and largely dispersed the valence band top. Combining the crystal structure and the electronic structure, M is expected to be a reduction site, whereas the oxidation could occur at either a Bi or an O site in the Bi-M-O complex photocatalysts.[72] Then the photocatalytic performance of the Bi-M-O compounds would exhibit significant difference at different lattice planes, along with the varied density of the Bi, M and O atoms at different lattice planes.

Although the $BiVO_4$ and Bi_2MO_6 (M=Mo, W) photocatalysts have a similar configuration of the band structures, the band positions were different because of their different chemical composition and crystal structures. Knowledge of the band positions is useful in as much as they indicate the thermodynamic limitations for the photoreactions that can be carried out with the photogenerated charge carriers. Therefore, it is important to clarify the band edge potentials of the photocatalyst. For a M_aN_b compound, the conduction band edge can be predicted by the following equation:[73, 74]

$$E_{CB} = (X_M{}^a X_N{}^b)^{1/(a+b)} - E^c - 1/2E_g + 0.059(pH_{ZPC} - pH) \quad (1)$$

where X_M and X_N are the absolute electronegativity of the atoms M and N respectively, which is defined as the arithmetic mean of the atomic electron affinity and the first ionization energy; E^c is the energy of free electrons on the hydrogen scale (about 4.5 eV); E_g is the band gap of the semiconductor; and pH_{ZPC} is the point of zero charge. The estimated E_{CB} at pH_{ZPC} by the above equation for $BiVO_4$, Bi_2MoO_6 and Bi_2WO_6 is about 0.45 eV, 0.51 eV and 0.52 eV respectively (Fig. 2) using the Pearson Absolute Electronegativity.[75]

The low conduction band level of the $BiVO_4$, Bi_2MoO_6 and Bi_2WO_6 photocatalyst indicates the insufficient reduction power of the photogenetated electrons with electron acceptors such as O_2. For the single-electron reduction of oxygen ($O_2 + e^- \rightarrow \cdot O_2^-$ (aq)), the standard redox potential is about -0.284 V vs. NHE which is much negative than the E_{CB} of $BiVO_4$, Bi_2MoO_6 and Bi_2WO_6 photocatalyst. This could increases the recombination rates of electron–hole pairs. Then the most effective approaches to improve the photocatalytic performance of the Bi-M-O photocatalysts are based on decreasing the recombination rate of photogenerated charge carriers. According to the predicted E_{CB}, the E_{VB} of the $BiVO_4$, Bi_2MoO_6 and Bi_2WO_6 is estimated at 2.85 eV, 3.1 eV and 3.27 eV respectively. It is clear the valence band position of Bi_2WO_6 is more positive than $BiVO_4$ and Bi_2MoO_6, indicating a higher photo-oxidation ability. For this predominance, the Bi_2WO_6 photocatalyst usually exhibited better performance than the $BiVO_4$ and Bi_2MoO_6 on the photocatalytic oxidation of various organic contaminants.

Besides the band edge position, the different effective mass of charge carriers is another important factor leading to the different photocatalytic efficiency. It is known that the electronic effective mass is inversely proportional to the curvature of

conduction bands.[76] Dai's group compared the CB bottoms of Bi_2WO_6 and Bi_2MoO_6 by DFT calculations.[77] It was found the CB bottom of Bi_2WO_6 has larger curvature than Bi_2MoO_6, indicating a smaller electronic effective mass. The smaller effective mass of electrons for Bi_2WO_6 benefits to the separation and migration of photogenerated carriers and also resulted in better photocatalytic performance than Bi_2MoO_6.

3. Strategies to enhance photocatalytic properties

As described in section 1, $BiVO_4$, Bi_2WO_6 and Bi_2MoO_6 are highly promising photocatalysts for use in environmental purification and solar water oxidation. The major limiting factor on improving their photocatalytic activity is the excessive electron-hole recombination. Recently, many efforts have been made to address this problem, which include morphology control, surface optimization, doping and construction of composite material. This section will give an overview of each of these strategies and discuss how these strategies affected the photocatalytic performance.

3.1 Structure and morphology control

The photocatalytic activity is closely related to the size, morphology, and crystallinity of the photocatalysts. Controlling the microstructure of the photocatalysts provides an effective way to enhance their photocatalytic properties.

Nanostructured photocatalyst usually exhibited excellent photocatalytic activity, because the photocatalytic behavior is closely related to their particle size. For randomly generated charge carriers, the average diffusion time from the bulk to the surface is given by $\tau=r^2/\pi^2D$, where r is the grain radius and D is the diffusion coefficient of the carrier.[78] If the grain radius decreases, larger numbers of

photogenerated charge carriers will transfer to the surface for photocatalytic reaction. It has been reported the nanoscale $BiVO_4$, Bi_2WO_6 and Bi_2MoO_6 exhibited much enhanced photocatalytic activity than that of their bulk samples obtained by solid state reaction.[79-82] In a recent study, Colón et al. prepared several $BiVO_4$ samples with different morphologies, such as peanut-like and needle-like architectures. It was found the photocatalytic activity of the prepared $BiVO_4$ is strongly affected by the crystallite size and morphology, and the needle-like $BiVO_4$ with smaller crystallite size exhibited better photocatalytic performance.[83]

Because of the layered crystal structure, plate-like morphology is a primary nanostructure for the $BiVO_4$, Bi_2WO_6 and Bi_2MoO_6 photocatalyst. Yu et al. compared the photocatalytic activity of two dimensional (2D) nanostructures with other morphology.[84] In their studies, the 2D (disclike and platelike) $BiVO_4$ demonstrates better photocatalytic activity than 3D and bulk $BiVO_4$. Especially, the $BiVO_4$ nanoplate exhibited the highest photocatalytic activity on degradation of RhB. Zhu's group systematically studied the reasons for the excellent photocatalytic activity of Bi_2WO_6 nanoplates,[71,85,86] which is ascribed to the large BET surface area and the thin thickness of the laminar structure.

Though minimizing the particle size could effectively enhance the photocatalytic activities, the decreased particle size makes it harder to be separated and recycled from the treated waste water in industrial use. Nano-/micro-sized hierarchical structures integrate the virtues of nanoscale and micro-scale. Most of the recent studies on the morphological control of the $BiVO_4$, Bi_2WO_6 and Bi_2MoO_6 photocatalysts were focused on hierarchical structures. Hierarchical structured $BiVO_4$ has been reported exhibited dendrite,[87-89] flower-like[90] and olive-like morphology etc (as shown in Fig. 3).[91-93] They exhibited excellent photocatalytic activity because of

their unique morphology.[89,91,93] Flower-like Bi_2WO_6 and Bi_2MoO_6 microspheres are usually obtained when they are hydrothermally synthesized (as shown in Fig. 4).[94,95,96,97-107] The diameter of the flower-like microspheres is in the range of micrometers. Studies on the formation mechanism have indicated that these flower-like hierarchical structures are built from oriented aggregation of two-dimensional Bi_2WO_6 nanoplates with a thickness and average length in nanoscale.[95,97] Compared with bulk samples obtained by solid state reaction, these flower-like Bi_2WO_6 microspheres exhibited much higher photocatalytic activity on the degradation of various organic contaminants, such as RhB,[95,97] acetaldehyde,[99] and Orange-II.[101] Recently, Amano et al. studied the effects of hierarchical architecture on the photocatalytic activity of Bi_2WO_6.[108] It was found the high photocatalytic activity did not depend on the assembling morphology of flakes. For Bi_2WO_6 samples of similar W/Bi ratio, the photocatalytic activity increased with an increase in their specific surface area. They hypothesize that both a small density of recombination centers and a large specific surface area are essential factors for a high photocatalytic activity.

Because of the large specific surface area, porous nanostructure has been extensively studied recently. Mesoporous monoclinic $BiVO_4$ (Fig. 5a) prepared by Yu et al. with a high BET surface area of 59 m^2g^{-1} exhibited a superior visible light-driven photocatalytic activity for the methylene blue degradation and NO oxidation.[109] The enhanced activity is due to its physicochemical properties such as crystal size, BET surface area, and porous structure, which not only supplies more active sites for the degradation reaction but also effectively promotes the separation efficiency of the electron-hole pairs.[109] The advantages of ordered porous structure for photocatalysis were further proved by studying the photocatalytic performance of

ordered macroporous Bi_2WO_6 (Fig. 5b,c).[110,111] It was believed the excellent photocatalytic activities were related to the improved light-harvesting properties, as well as the continuous porous structure.

3.2 Surface optimization and modification

The photocatalytic degradation of a pollutant must proceed at the surface of the photocatalyst, and consequently the surface properties appear as an important parameter. It was reported when the monoclinic $BiVO_4$ photocatalyst (JCPDS file No.14-0688, space group: I2/a, a=5.195, b=11.701, c=5.092) exposes more facets of {010}(as shown in Fig. 6a,b), it exhibited greatly enhanced photocatalytic activity.[112-114] The high photocatalytic activity may be ascribed to the larger atom density of the {010} facets (as shown in Fig. 6c) on the exposed surfaces, which is beneficial to the adsorption and degradation of the pollutants.[112,113] Density functional theory calculations by Li et al. studied the surface properties of monoclinic $BiVO_4$.[115] The calculated results indicated in all of the most stable terminated planes of $BiVO_4$, the V atoms are fully coordinated, and all of the dangling bonds are derived from the broken Bi-O bonds. A dangling bond plays an important role in the surface adsorption properties. The {010} facets is thermodynamically lowest-energy surface of monoclinic $BiVO_4$. The high density of cleaved Bi-O bonds in {010} facets may improve the adsorption property on the surface, which is advantageous for the photocatalytic reaction. On the other hand, considering that the photocatalytic oxidation of contaminant would occur at either a Bi or an O site in the $BiVO_4$ photocatalysts, the larger atom density of Bi and O in {010} facets could also improve the photocatalytic efficiency.

The photocatalytic activity of preferential oriented $BiVO_4$ was also investigated by Ye' group.[116] They found the high photocatalytic activity of (001) plans resulted from

their superior hydrophilic ability. The similar viewpoint was proposed by Skrabalak et al. in their studies on the structure-dependent photocatalytic properties of Bi_2WO_6.[117] It was found that the enhanced performance of the Bi_2WO_6 microspheres is partially ascribed to bismuth-rich hydrophilic surface.

Saison et al. established a relationship between surface acidity and photocatalytic performance on RhB degradation in Bi_2O_3, $BiVO_4$ and Bi_2WO_6 materials.[118] It was found the best photocatalytic performance for contaminants degradation was obtained with the Bi_2WO_6 sample that also exhibits the highest surface acidity. The most acid sites may promote a strong interaction with the pollutant, implying a short distance between the pollutant and the photocatalyst. Consequently, the photogenerated electrons, holes, and radicals can reach more easily to the pollutant, leading to an efficient degradation under visible light.

Surface fluorination is an effective method for modifying the surface property of oxide photocatalysts and then improving their photocatalytic performance. Zhu et al. synthesized fluorinated Bi_2WO_6 photocatalyst by a simple hydrothermal process.[119] They found the fluorination of Bi_2WO_6 affected not only the reaction rate but also the mechanistic pathways of the RhB degradation. The fluorinated Bi_2WO_6 exhibited enhanced photocatalytic activity for the RhB degradation. More RhB molecules were degraded via the de-ethylation process by the fluorinated Bi_2WO_6 (as shown in Fig.7). It was proposed that the F-containing function on the catalyst surface could serve as an electron-trapping site and enhance interfacial electron-transfer rates by tightly holding trapped electrons. As a result, more RhB molecules were degraded via the N-demethylation process.[119] Yu et al. studied the surface fluorinated $BiVO_4$ photocatalyst synthesized by NaF-mediated hydrothermal processes.[120] It was found the surface fluorination favored the RhB adsorption and hole transfer between RhB

molecules and $BiVO_4$ photocatalyst, thus progressively enhancing the initial direct hole transfer mediated de-ethylation process.

In a recent study by Luo et al., surface pretreatment by electrochemical cyclic voltammetry (CV) in the dark was found could remarkably enhance the photocurrent of Mo-doped $BiVO_4$ from the front side illumination.[121] Fig. 8 illustrated the possible mechanism for the enhanced photocurrent. Some MoO_x segregation precipitated on the surface of the Mo-doped $BiVO_4$ electrode during the preparation of the photoelectrode. MoO_x acts as a recombination center and has a negative effect on the photocurrent. After the pretreatment, MoO_x on the surface was dissolved into the electrolyte, improving the separation and transfer of the photogenerated charge carriers.

3.3 Doping

Previous studies have reported that doping impurities into a semiconductor can improve photocatalytic performance. However, the effect of doping may not always be advantageous. There are two kinds of dopant levels, including deep level and shallow level. A deep level usually acts as a recombination center, severely decrease the photocatalytic activity. Therefore, appropriate dopants and their concentrations are important to increase the performance of the photocatalysts. In this section, a few types of dopants that were reported to enhance the photocatalytic performances of $BiVO_4$, Bi_2WO_6 and Bi_2MoO_6 are reviewed and their roles are examined.

Since Ye et al. found the photocatalytic activity of $BiVO_4$ for O_2 evolution and methylene blue (MB) degradation under visible light irradiation was evidently improved by 2 atom% Mo doping,[122] metal doped $BiVO_4$ has been obtained increasingly attention by many research groups. In the studies by Ye's group, they proposed the improved adsorption affinity towards electrolytes or organic molecules

was an important reason for the enhanced activity of Mo doped $BiVO_4$, due to its higher surface acidity than pure $BiVO_4$. The surface acidity of $BiVO_4$ is possibly increased by Mo ion substitution, since Mo^{6+}ion has a larger electronegativity than that of V^{5+}. Therefore, the role of Mo doping is thought as affecting the adsorption affinity rather than the photo-oxidation ability in determining the photocatalytic activity of the photocatalyst.

Zou's group further studied the Mo doped $BiVO_4$ for photoelectrochemical hydrogen generation from seawater.[123] The Mott–Schottky method was used to investigate the donor concentration of the Mo-doped $BiVO_4$, which can be calculated by the slope of the Mott-Schottky curves. It was found the carrier concentration increased about 80 times after doping with Mo (Fig. 9), indicating a high conductivity.

In order to identify effective dopants for $BiVO_4$ more rapidly, Bard's group performed rapid screening of $BiVO_4$ photocatalysts doped with various metals (W, Fe, B, Cu, Zn, Ti, Nb, Sn, Co, Pb, Rb, Ru, Ag, Ga, Sr, and Ir) using a scanning electrochemical microscopy (SECM) technique.[124] Among the elements they have tried, only addition of 5-10% W showed noticeable enhancement of photocurrent. The Bi/V/W oxide with a 4.5:5:0.5 ratio exhibited the highest photocurrent under UV -visible and visible light irradiation. Addition at 10 to 20 % levels of elements like Sn, Co, Pd, Rb, Ru, Ag, Ga, Sr, and Ir showed a negative effect and the others basically showed the same behavior as the Bi/V oxide. Mott–Schottky plots revealed that the majority carrier level in the W-doped sample increased approximately 2 times. The increase of the doping level with a decrease in the resistance of the material is probably a contributing factor in the enhanced photocurrent of the Bi/V/W (4.5/5/0.5) oxide. Using the same technique, Park et al. demonstrated that W/Mo co-doped

$BiVO_4$ (Bi: V: W: Mo atomic ratio of 4.6: 4.6: 0.2: 0.6) had 10 times higher photocurrent than undoped $BiVO_4$. No changes in band gap of W-doped $BiVO_4$ and W/Mo-doped $BiVO_4$ were observed, while the increase in carrier density was confirmed by the decrease in the slope of the Mott–Schottky plots. Furthermore, deformation of crystal structure of the scheelite $BiVO_4$ occurs with consecutive doping of W and Mo. It was found the crystal symmetry shifted from monoclinic to tetragonal. W and Mo in this study are revealed as excellent shallow dopants, which facilitate the separation of photogenerated electron-hole pairs and effectively increase the charge carrier density of $BiVO_4$ photocatalyst.[125]

Mullins et al. also studied the Mo-, W- and Mo/W-doped $BiVO_4$ electrodes by ballistic deposition (BD).[126] They found the optimal levels for individual incorporation were 2.5% W and 5% Mo, which resulted in photocurrent densities that were 7 and 8 times higher than that of pure $BiVO_4$, respectively. Further improvement was observed for co-incorporation of Mo and W. The optimal level for co-incorporation was also found to be 6% Mo and 2% W, which exhibited a photocurrent density that was 10 times higher than that of pure $BiVO_4$.

Recently, Luo et al. systematically studied the effect of doping on $BiVO_4$ with higher valence metal ions (Mo^{6+}, $W^{6+}$and Sn^{4+}) at V^{5+} and Bi^{3+} sites by DFT calculation and photoelectrochemical measurements.[127] It was found Mo or W could substitute V sites, but Sn did not substitute Bi sites because of a higher formation energy and lower solubility of impurity ions, leading to serious SnO_2 segregation on the surface. Therefore, Mo^{6+}or W^{6+}-doped $BiVO_4$ exhibited a much higher photocurrent while the photocurrent of Sn^{4+}-doped $BiVO_4$ did not change obviously. Moreover, they found the surface segregation of the doping ions had a negative effect on the performance in the doped samples. Therefore, for an n-type semiconductor

photoelectrode, doping with a metal ion with higher valence, lower formation energy and less surface segregation can improve the photoelectrochemical performance.

To integrate the advantages of both Bi_2WO_6 (high photocatalytic activity) and Bi_2MoO_6 (narrower band gap), many researchers have studied the W^{6+} doped Bi_2MoO_6 or Mo^{6+} doped Bi_2WO_6. From a structural viewpoint, Bi_2WO_6 is isostructural with Bi_2MoO_6. It could be expected that the substitution of W^{6+} and Mo^{6+} with each other may produce a stable $Bi_2Mo_xW_{1-x}O_6$ solid solution, because of the structural similarities between the cations, thus leading to improved properties. Actually, phase-pure $Bi_2Mo_xW_{1-x}O_6$ photocatalysts have been successfully synthesized by many research groups and their enhanced visible-light-driven photocatalytic activities were demonstrated.[128-131] For instance, $Bi_2Mo_xW_{1-x}O_6$ solid solutions with various compositions (x= 0, 0.25, 0.50, 0.75, and 1.00) have been prepared by Yu's group via hydrothermal treatments.[128] For the $Bi_2Mo_xW_{1-x}O_6$ solid solutions with x = 0.25, 0.50, and 0.75, valence band spectra from XPS indicate the valence band is widened and elevated when compared with the pure Bi_2WO_6 photocatalyst, leading to the narrower band gaps of the $Bi_2Mo_xW_{1-x}O_6$ solid solutions (x = 0.25, 0.50, and 0.75) . The $Bi_2Mo_{0.25}W_{0.75}O_6$ sample with a relatively high W content exhibited the highest photocatalytic activity on the degradation of MB. Zhu's group reproduced the phase-pure $Bi_2Mo_xW_{1-x}O_6$ solid solutions (x =0, 0.05, 0.25, 0.5, 0.75, 0.95, 1) and studied the effects of Mo replacement on the structure and visible-light-induced photocatalytic performances.[129] Theoretical calculations based on density functional theory revealed introduction of Mo atom into Bi_2WO_6 could reduce the conduction band level of Bi_2WO_6 and the curvature of the conduction band. Under visible light irradiation (λ>420 nm), Bi_2WO_6 showed relatively higher photocatalytic activity than other samples. However, under visible light λ > 450 nm,

$Bi_2Mo_{0.25}W_{0.75}O_6$ shows much higher activity than Bi_2WO_6. They assumed the higher efficiency of Bi_2WO_6 under visible light $\lambda > 420$ nm was attributed to more effective photoelectron transfer in the conduction band with larger curvature, while the higher performance of $Bi_2Mo_{0.25}W_{0.75}O_6$ under visible light $\lambda > 450$ nm was attributed to its lower band gap compared with Bi_2WO_6.

Different from the inter-replacement of W^{6+} and Mo^{6+}, the substitution of M (M=W, Mo) sites with other different ions in Bi_2MO_6 (M=W, Mo) might induce a slight modification of crystal structure due to the different ion radii, resulting in dramatic influence on the mobility of the charge carrier and then change the photocatalytic and photophysical properties. For instance, we prepared Zr^{4+} doped Bi_2WO_6 by substituting the W^{6+} ions in the crystal lattice.[132] Because of the lower valence states of Zr, the substitution of W^{6+} by Zr^{4+} lead to an extrinsic oxygen vacancy (Vo) by charge compensation effect. The presence of Vo in the zirconium doped sample was confirmed by XPS analysis. The positively charged oxygen vacancy defects can improve oxygen adsorption and function as electron acceptors to reduce the recombination of charge carriers and then increase the photocatalytic performance. Lai et al. studied the influence of Vo on the electronic band structures of Bi_2MO_6 (M=W, Mo) with one Vo by means of density functional theory (DFT).[77] It was found Vo in Bi_2MO_6 (M= W, Mo) introduced localized W 5d or Mo 4d states in band gap, which may serve as a trapping center of photogenerated electrons and consequently improve photocatalytic oxidation performance.

Nonmetal elements doped samples were also studied to obtain a high-performance photocatalyst. For instance, F-substituted Bi_2WO_6 ($Bi_2WO_{6-X}F_{2X}$) photocatalysts were successfully synthesized by Zhu's group.[133] It was found that F-substitution could change the original coordination around the W and Bi atoms. Density functional

calculations revealed that $Bi_2WO_{6-X}F_{2X}$ possesses a wider valence bandwidth and lower valence band position, resulting in an increased mobility of photo-generated charge carriers and a stronger oxidation power. For this reason, the photocatalytic activity of $Bi_2WO_{6-X}F_{2X}$ increased about 2 times compared with pure Bi_2WO_6 on the degradation of MB under visible-light ($\lambda > 420$ nm) irradiation. Another example for nonmetal doped Bi_2WO_6 by the substitution of O atoms is N doped Bi_2WO_6.[134] Our research group studied the effects of nitrogen doping on the crystal structure, optical properties, and photocatalytic performance experimentally. The results showed that the doped samples exhibit 2–3 times higher photocatalytic activities than the undoped one, which was strongly dependent on the N-doping level. The sample with the atomic ration of N to Bi of 0.5 exhibited the best photocatalytic activity. Close investigation revealed that doping Bi_2WO_6 with N could not only enhance the visible light adsorption, but also improve the charge separation and transfer, which may be the reason for the significantly enhanced photocatalytic activities. Dai's group studied the N doped Bi_2WO_6 by DFT calculations.[77] From the calculated results (as shown in Fig. 10), it was found the substitution of N for O induces hybrid states of O 2p and N 2p near the top of valence band, leading to the increases of the VB width and the decreases of band gap. This study theoretically proved the increased mobility of photo-generated charge carriers, the enhanced visible-light absorption property, and the origin of the improved photocatalytic behavior of N doped Bi_2WO_6.

3.4 Construction of composite material

Construction of composite photocatalysts provides an interesting way to increase the photocatalytic performance by decreasing the charge recombination and extending the light response of photo-excitation. In this section, a few types of composite materials and the fundamentals for their improved photocatalytic activity will be reviewed.

3.4.1 Composite with semiconductor

Semiconductor-based composite material with a heterojunction structure has been extensively studied for obtaining a high-performance photocatalyst. When heterojunctions constituted by semiconductors with matching band potentials, photogenerated charge carriers can transport from one semiconductor to another driven by the contact electric field, leading to efficient separation of photogenerated electron-hole pairs. For a particulate $BiVO_4$ composite material, it has been reported the photocatalytic performance could be improved by compositing with Co_3O_4,[74,135] V_2O_5,[136,137] CeO_2,[138] Bi_2O_3,[139,140] Bi_2S_3,[141] CuO[142] and Cu_2O[143] et al. Long et al. studied the mechanism for the improved photocatalytic activity of the $Co_3O_4/BiVO_4$ composite material with a p-n heterojunction structure.[74,135] The band edge position of the Co_3O_4 and $BiVO_4$ were estimated from the absolute electronegativity (equation 1). According to the band edge position, the excited electrons on the conduction band of the p-type Co_3O_4 could transfer to that of the n-type $BiVO_4$, and simultaneously holes on the valence band of n-type $BiVO_4$ can be transferred to that of p-type Co_3O_4 under the potential of the band energy difference. This process decreased the recombination rate of electron-hole pairs. The similar mechanism for the improved photocatalytic performance that the heterojunctions promote the separation of photogenerated electron–hole pairs was further confirmed in the $V_2O_5/BiVO_4$, $Bi_2O_3/BiVO_4$, $Bi_2S_3/BiVO_4$ and $Cu_2O/BiVO_4$ composites.[137,139-141,143]

Su et al. employed surface photovoltage spectroscopy (SPS) and transient photovoltage (TPV) techniques to investigate the effect of heterojunction structure on the behavior of photogenerated charges in $V_2O_5/BiVO_4$ composite material.[137] Fig.11a is the TPV spectra of bare $BiVO_4$, bare V_2O_5, and the 5.3 wt % $V_2O_5/BiVO_4$ composite. A positive TPV spectrum of V_2O_5 implies that positive charges accumulate

on the V_2O_5 surface at the top electrode under irradiation, while the negative sign of $BiVO_4$ is attributed to negative charge accumulation on the surface. Different from bare V_2O_5 and $BiVO_4$, the $V_2O_5/BiVO_4$ composite semiconductor shows an initial negative response and next positive response reversed at 7×10^{-6}s in the TPV spectrum. For the $V_2O_5/BiVO_4$ composites, the intensities and lifetime of the TPV response are much improved compared with those of the bare $BiVO_4$ and V_2O_5. These TPV features of $V_2O_5/BiVO_4$ can be ascribed to the improved charge separation o in the composite structure, as shown in Fig. 11b.

$BiVO_4/WO_3$ composite photoanode films were widely studied for its excellent performance on water splitting.[144-146] The heterojunction structure provided enhanced photoconversion efficiency due to the improved charge separation in the composite structure.[144-146] The WO_3 layer played as barrier for the holes of $BiVO_4$ to reach FTO surface, which decreased the electron-hole recombination and caused the efficient water oxidation.[146]

Saito and coworkers deposited a SnO_2 layer between WO_3 and $BiVO_4$ to further improve the photoconversion efficiency of the $FTO/WO_3/BiVO_4$ film.[147] The effect of a SnO_2 layer has been discussed in a $FTO/SnO_2/BiVO_4$ photoanode film by van de Krol's group before.[148] They found a SnO_2 layer could act as a hole mirror that prevents recombination via FTO-related defect states at the $FTO/BiVO_4$ interface (Fig. 12a). This approach promoted the charge collection and greatly improved the external quantum efficiency (IPCE) of the $BiVO_4$ films (as shown in Fig. 12b).

Bi_2WO_6/TiO_2 has been widely studied due to its much enhanced photocatalytic performances.[149,150-158] The VB position of TiO_2 is higher than that of Bi_2WO_6. When the TiO_2 coupled with Bi_2WO_6 to form a semiconductor heterojunction, photo-generated holes from the VB of Bi_2WO_6 would transfer to the VB of TiO_2,

efficiently suppressing its recombination with photo-generated electrons from the Bi_2WO_6 photocatalyst. Therefore, Bi_2WO_6/TiO_2 composite material exhibited much enhanced photocatalytic activity on degradation of various contaminants, such as stearic acid,[158] acetaldehyde,[149] rhodamine B (RhB),[149,150,155] methylene blue (MB),[154,157] NH4+/NH3,[152] and Brilliant Red X3B.[153]

Besides the Bi_2WO_6/TiO_2 composite, it has been reported the photocatalytic performance of Bi_2WO_6 could be evidently improved by coupling with Bi_2O_3,[159-162] C_3N_4,[163,164] WO_3,[165] Co_3O_4,[166] CdS,[167] ZnO,[168] $ZnWO_4$,[169] and Bi_2S_3[170] et al. There is some different from TiO_2/Bi_2WO_6 composite when the Bi_2WO_6 coupled with Bi_2O_3, C_3N_4, WO_3, Co_3O_4, CdS and Bi_2S_3. These semiconductors could be excited under visible light irradiation. Besides the effective charge separation from their heterostructure, the improved photocatalytic performance in these systems is inevitably associated with the extended energy response of photo-excitation, leading to enhanced charge carriers generation under visible light irradiation.

3.4.2 Composite with carbon material

Carbon materials, such as graphene oxide (GO), C_{60}, carbon quantum dots, carbon nanotube, carbon spheres and carbon nanofibers, have been used to composite with $BiVO_4$ and Bi_2MO_6 (M=W, Mo) photocatalysts to improve their photocatalytic performance.[171-185] Among these carbon materials, GO composite materials obtained the most attention recently, owing to its perfect conjugated sp^2-hybridized carbon structure and large BET surface area. The conjugated sp^2-hybridized structure provides abundance of delocalized electrons to enhance the transport of photo-generated electrons. The large BET surface area could increase the adsorption of target molecules. Both of these two predominance lead to an increase in the photo-conversion efficiency of GO composited photocatalyst. $BiVO_4$-RGO composite

prepared by Ng et al. proved the predominance of RGO for efficient photocatalytic splitting.[172] A remarkable 10-fold enhancement in photoelectrochemical water splitting reaction is observed. A recent study for a composite material of RGO and Bi_2WO_6 quantum dots (QDs) (as shown in Fig. 13a) in our group also proved the advantage of RGO as a base material to improve the photocatalytic performance.[174] Electrochemical measurements indicated the electron conductivity is largely improved in the RGO-Bi_2WO_6 QDs composite. The electron lifetime in the RGO-Bi_2WO_6 QDs composites was increased 8-fold compared with that of the pure Bi_2WO_6 QDs. The tightly anchored interface facilitates the electron transfer from Bi_2WO_6 to RGO, leaving most of the photo-generated holes on the Bi_2WO_6 surface to take part in photo-oxidation reactions (Fig. 13b). Ma et al. investigated the influence of RGO amount on the photocatalytic activity in the RGO/Bi_2WO_6 composite material.[177] It was found the optimum amount of RGO is 20 mg for 1 mmol Bi_2WO_6, at which the RGO/Bi_2WO_6 sample displays the highest reactivity. Zhou et al. prepared RGO/Bi_2MoO_6 composites with a RGO content from 0.5 to 4.0 wt%.[178] Their studies indicate the photocatalytic activities of the RGO/Bi_2MoO_6 composites were dependent on the amount of graphene and it was found that the optimal hybridized amount of graphene was about 1.0 wt%. Similar with GO, the delocalized conjugated electrons in C_{60} and carbon nanotubes could also increase the photogenerated electron transfer in their composite material to reduce electron-hole recombination and enhance the photoconversion efficiency, as reported in the C_{60}/Bi_2WO_6,[180] C_{60}/Bi_2MoO_6[184] and carbon nanotube/$BiVO_4$[173] composite materials. Besides the crystalline carbon material, amorphous carbon such as carbon spheres, carbon dots and carbon nanofibers composited Bi_2MO_6 (M=W, Mo) were also reported exhibited improved photocatalytic activity.[181-183] These studies revealed the enhanced specific

surface area and the effective separation of the photogenerated carriers in the composite material is responsible for their improved photocatalytic activity.

3.4.3 Metal loaded

Noble metals, such as Ag, Pt, Au and Pd, have been used as electron acceptors to increase the separation of the photo-generated hole/electron pairs and promote interfacial charge-transfer. It has been reported the noble metal loaded $BiVO_4$ and Bi_2MO_6 (M=W, Mo) photocatalysts exhibited enhanced photocatalytic activities on contaminants degradation and water oxidation.[186-192] Cao et al. studied the effect of noble metal on the photocatalytic process in detail in Au-$BiVO_4$ heterogeneous nanostructures.[186] Their studies revealed the gold-enhanced photocatalytic efficiencies are attributed to two reasons. First, the surface loaded gold nanoparticles may act as electron acceptors to decrease the recombination rate of the photogenerated electrons and holes. From the energy diagram of the Au-$BiVO_4$ junction (Fig. 14), it can be clearly seen the photo-generated electrons is prone to transfer into the Au nanoparticle because of its lower Fermi level when comparing with the CB potential of $BiVO_4$. Such a charge transfer process enhances the separation of photogenerated electrons and holes and thereby increases their lifetime. This is particularly important for photocatalytic water oxidation because it is a slow multi-electron process with kinetic restraints.[193] Second, the SPR effect of gold nanoparticles on $BiVO_4$ surfaces can also contribute to the improved visible light photocatalytic efficiency. To clarify this viewpoint, they compared the photocatalytic activity of Au-$BiVO_4$ with Pt-$BiVO_4$ nanosheets and pure $BiVO_4$ under irradiation of 500 ± 20 nm light. The results indicate the much higher photocatalytic activity of Au-$BiVO_4$ is arrived from the strong SPR at 500 ± 20 nm. It is believed that the gold SPR can enhance the electron−hole separation near the Au-$BiVO_4$ heterojunction, and thus improve the

photocatalytic efficiency. Our recent studies indicated Ag-loaded Bi_2WO_6 photocatalysts exhibited significantly enhanced photocatalytic activity in inactivating E. coli , a Gram-negative bacterium, and S. epidermidis, a Gram-positive bacterium under visible light irradiation (λ> 420 nm).[187]

3.4.4 Co-catalyst loaded

A co-catalyst was usually coupled with a photocatalyst to increase the photo-conversion efficiency and to improve the stability of the photocatalyst, especially in a photocatalytic water splitting process. Oxygen evolution is kinetically the key step in the photocatalytic water splitting. Cocatalysts could lower the activation potential for O_2 evolution. Besides, lots of studies have revealed hole accumulation at the photoanode/electrolyte interface often results in photocorrosion,[194,195] and a cocatalyst could increase the stability for O_2 evolution. For $BiVO_4$ photoanodes as an instance, Sayama et al. found the surface V atoms dissolved from the bare $BiVO_4$ surface during the photoreaction,[194] inducing a significantly decreased photocurrent within a few minutes. To solve this problem, they attempt to modify the surface of $BiVO_4$ with Ag^+ ions, which involved simply dipping the $BiVO_4$ electrode in an $AgNO_3$ solution. Although the exact form of the responsible species was not identified, the Ag-modified $BiVO_4$ electrode exhibited enhanced O_2 evolution and noticeably improved stability. They surmised the Ag+ ion in/on the $BiVO_4$ catalyzed the intrinsic photogeneration of oxygen with the holes. Recently, various cocatalyst have been combined with $BiVO_4$ to enhance the O_2 evolution while reducing photocorrosion.

Up to the present, the most commonly used cocatalyst to improve water oxidation kinetics of $BiVO_4$ or doped $BiVO_4$ photoanodes was Co-Pi.[196-202] CoPi have been demonstrated to work effectively as oxygen-evolving electrocatalyst (OEC) at pH 7

buffered with aqueous phosphate in electrolysis.[203] When catalyzing water oxidation, Co-Pi undergoes proton-coupled electron transfers along with cyclic valency changes between Co (II/III) and Co (III/IV).[204] In photoelectrolysis, it has been demonstrated the primary role of CoPi is to inhibit charge recombination by facilitating the hole transfer via the cobalt ion valency cycle.[200] For Co-Pi modified W:$BiVO_4$ as an example, Zhong et al. found Co-Pi deposition yields a remarkable ~440 mV cathodic shift in the onset potential for sustained PEC water oxidation at pH 8. [196] The much lower absolute onset potential is promising for solar water splitting in low-cost tandem PEC cells. Moreover, the PEC current of Co-Pi modified W:$BiVO_4$ is about three times higher than that of the parent W:$BiVO_4$ photoanode. Almost completely suppress of surface electron-hole recombination by Co-Pi addition was observed in their studies. They summarized the mechanism of Co-Pi on inhibition of the surface electron-hole recombination, as shown in Fig. 15. For bare W:$BiVO_4$, surface recombination (J_{sr}) is a major loss pathway which results in poor water oxidation (J_{ox}) and poor PEC photocurrent densities. After Co-Pi modification, almost all of the photogenerated holes that migrate to the W:$BiVO_4$ surfaces can be captured by the Co-Pi electrocatalyst to oxidize water with nearly quantum efficiency. Obviously, Co-Pi deposition provides a facile route by which photogenerated holes can be captured and used in the productive four-electron oxidation of water. Co-Pi modified Mo-doped $BiVO_4$ electrode prepared by Pilli et al. exhibited a similar superior PEC characteristics in terms of onset potential and photocurrent density.[197] Furthermore, it was found the Co-Pi/Mo-doped $BiVO_4$ photoelectrode exhibited better stability as compared to bare Mo-doped $BiVO_4$ electrode under photolysis conditions.

For the same attempt to enhance O_2 evolution and reduce photocorrosion, Seabold et al. coupled the $BiVO_4$ photoanode with a different type of cocatalyst, FeOOH

which is also a O_2 evolution electrocatalyst.[195] They found the $BiVO_4$/FeOOH films generated remarkably improved photocurrent for water oxidation, which is comparable to photocurrent generated by bare $BiVO_4$ using sulfite as the hole scavenger, verifying the ability of FeOOH to efficiently collect photogenerated holes from the $BiVO_4$ layer and facilitate water oxidation to O_2. The effect of FeOOH on the photostability of $BiVO_4$ was also examined in their study. It was found the photocurrent generated by the bare $BiVO_4$ film decreased significantly within a few minutes because of the anodic photocorrosion. When the FeOOH layer was added to the surface of the $BiVO_4$ electrode, a much enhanced photocurrent density was maintained for 6 h with only 2% of decay. This result demonstrates the exceptional performance of FeOOH for improving photostability as well as photocurrent of $BiVO_4$ in PEC water oxidation. The photocurrent-to-O_2 conversion efficiency of the prepared $BiVO_4$/FeOOH photoanode is up to 96%.

Comparing with the photocatalytic water splitting, co-catalyst deposition was less focused on contaminant degradation. A typical study was recently reported by Lin et al. on Pt and RuO_2 co-loaded $BiVO_4$ (denoted as Pt-RuO_2/$BiVO_4$).[205] The Pt-RuO_2/$BiVO_4$ could oxide thiophene to SO_3 in acetonitrile solution under visible light irradiation with molecular oxygen as oxidant. A high photocatalytic activity of thiophene oxidation was achieved by only loading 0.03 wt% of Pt and 0.01 wt% of RuO_2 as dual co-catalysts on $BiVO_4$. In Pt-RuO_2/$BiVO_4$, Pt acted as a reduction co-catalyst and RuO_2 acted as an oxidation co-catalyst. The co-existence of oxidation and reduction co-catalysts is beneficial for the efficient separation and transfer of the photo-excited electrons and holes, resulting in the high photo-catalytic activity of thiophene oxidation. Recently, Cu^0 was found as an excellent co-catalyst for Bi_2WO_6 photocatalyst in our research group.[206] The copper reagent not only served as a

heterogeneous catalyst to generate hydroxyl radicals by Fenton-like reaction, but also acted as an electron shuttle that facilitated the circulation of the photogenerated carriers to improve the photocatalytic performance.

4. Summary and Outlook

Over the past few years, the numerous efforts put on bismuth based complex oxide semiconductors have resulted in a rich database for their synthesis, properties, modifications, and photocatalytic applications. The mostly studied bismuth based complex oxide photocatalysts are $BiVO_4$, Bi_2WO_6 and Bi_2MoO_6 up to the present. This review summarized the structures, preparations and properties of these bismuth based photocatalysts for use in environmental purification and solar water oxidation, emphasizing the strategies that have been employed to enhance its photocatalytic properties. Although a significant improvement has been made for the development of highly efficient bismuth based complex oxides, there is still considerable problems for further investigated. The poor reduction power of the photogenetated electrons from the low conduction band edge potential resulted in the high recombination rates of photogenerated charge carriers, which is the main defect suppressing the photocatalytic performance of $BiVO_4$, Bi_2WO_6 and Bi_2MoO_6. Morphological control has significantly improved its photocatalytic performance by control of the crystallinity, BET surface, grain size and microstructure et al. It is worth to note decreasing the grain size would significantly decrease the bulk recombination rate of the photogenerated charge carriers. Quantum sized photocatalysts should be paid special attention in the future. However, the current synthesis methods are not sufficient for large-scale production of quantum sized photocatalyst. For this reason, further efforts must be made on the development of robust and reliable strategies for

fabricating various quantum sized photocatalysts. Surface control can be used to further improve the photocatalytic performance, considering the photocatalytic reactions proceed at the surface of the photocatalyst and only few of previous investigations were focused on the effect of crystal surface. This provides us with important research opportunities. We believe that the surface defects and configurations of surface atoms, but not limited to, should receive more attention in future studies. Preliminary investigations already show that photo-absorption and charge carrier separation could be improved by doping or construction of composite material. These investigations were mainly studied either experimentally or theoretically. More fundamental studies, combining the experiment, theory and calculation, are needed to help us to understand the photocatalytic principles. These research areas are ripe for growth. We will see an increasing number of new and novel progress of bismuth based complex oxides for application on environmental purification and solar water oxidation.

Acknowledgements

We acknowledge the financial support from the National Basic Research Program of China (2010CB933503, 2013CB933203), National Natural Science Foundation of China (51102262, 51272269), and the Science Foundation for Youth Scholar of State Key Laboratory of High Performance Ceramics and Superfine Microstructures (Grant No. SKL201204).

References

1 A. Fujishima and K. Honda, *Nature*, 1972, **238**, 37.

2 S. U. M. Khan, M. Al-Shahry and W. B. Ingler, *Science*, 2002, 297, 2243.

3 Z. Zou, J. Ye, K. Sayama and H. Arakawa, *Nature,* 2001, **414**, 625.

4 A. Kudo and Y. Miseki, *Chem. Soc. Rev.*, 2009, 38, 253.

5 K. Maeda, K. Teramura, D. Lu, T. Takata, N. Saito, Y. Inoue and K. Domen, *Nature,* 2006, **440**, 295.

6 A. J. Bard and M. A. Fox, *Acc. Chem. Res.*, 1995, **28**, 141.

7 F. E. Osterloh, *Chem. Mater.*, 2008, **20**, 35.

8 W. Choi, A. Termin and M. R. Hoffmann, *J. Phys. Chem.,* 1994, **98**, 13669.

9 R. Asahi, T. Morikawa, T. Ohwaki, K. Aoki and Y. Taga, *Science*, 2001, **293**, 269.

10 S. Sakthivel and H. Kisch, *Angew. Chem., Int. Ed.*, 2003, **42**, 4908.

11 W. Zhao, W. H. Ma, C. C. Chen, J. C. Zhao and Z. G. Shuai, *J. Am. Chem. Soc.*, 2004, **126**, 4782.

12 H. G. Kim, D. W. Hwang and J. S. Lee, *J. Am. Chem. Soc.*, 2004, **126**, 8912.

13 J. Sato, N. Saito, H. Nishiyama and Y. Inoue, *J. Phys. Chem. B*, 2001, **105**, 6061.

14 R. Abe, H. Takami, N. Murakami and B. Ohtani, *J. Am. Chem. Soc.,* 2008, **130**, 7780.

15 A. Hameed, T. Montini, V. Gombac and P. Fornasiero, *J. Am. Chem. Soc.,* 2008, **130**, 9658.

16 H. Gao, C. Liu, H. E. Jeong and P. Yang, *ACS Nano*, 2012, **6**, 234.

17 X. Zhou, H. Yang, C. Wang, X. Mao, Y. Wang, Y. Yang and G. Liu, *J. Phys. Chem. C*, 2010, **114**, 17051.

18 B. Hu, L. H. Wu, S. J Liu, H. B. Yao, H. Y. Shi, G. P. Li and S. H. Yu, *Chem. Commun.*, 2010, **46**, 2277.

19 Z. G. Zhao, Z. F. Liu and M. Miyauchi, *Chem. Commun.*, 2010, **46**, 3321.

20 A. Kudo, K. Omori and H. Kato, *J. Am. Chem. Soc.,*1999, **121**, 11459.

21 M. Wiegel, W. Middel and G. Blasse, *J. Mater. Chem.,* 1995, **5**, 981.

22 W. T. Fu, *Phys. C*, 1995, **250**, 67.

23 M. Oshikiri, M. Boero, J. Ye, Z. Zou and G. Kido, *J. Chem. Phys.*, 2002, **117**, 7313.

24 M. W. Stoltzfus, P. M. Woodward, R. Seshadri, J. H. Klepeis and B. Bursten, *Inorg. Chem.*, 2007, **46**, 3839.

25 C. Yin, S. Zhu, Z. Chen, W. Zhang, J. Gu and D. Zhang, *J. Mater. Chem. A*, 2013, **1**, 8367.

26 J. Yang , D. Wang, X. Zhou, C. Li, *Chem. Eur. J.*, 2013, **19**, 1320.

27 S. K. Choi, W. Choi and H. Park, *Phys. Chem. Chem. Phys.*, 2013,**15**, 6499.

28 C. Ding, J. Shi, D. Wang, Z. Wang, N. Wang, G. Liu and F. Xiong, C. Li, *Phys. Chem. Chem. Phys***.**, 2013, **15**, 4589.

29 S. K. Pilli, T. G. Deutsch, T. E. Furtak, L. D. Brown, J. A. Turner and A. M. Herring, *Phys. Chem. Chem. Phys.*, 2013, **15**, 3273.

30 H. S. Park, K. C. Leonard and A. J. Bard, *J. Phys. Chem. C*, 2013, **117**, 12093.

31 H. W. Jeong, T. H. Jeon, J. S. Jang, W. Choi and H. Park, *J. Phys. Chem. C*, 2013, **117**, 9104.

32 A. Kudo and S. Hijii, *Chem. Lett.*, 1999, 1103-1104.

33 C. Mao, M. Li, Z. Fang, F. Meng, X. Qu, Y. Liu, M. Wang, J. Zhang, Z. Shi and X. Guo, *RSC Adv.*, 2013, **3**, 6631.

34. J. Tian, Y. Sang, G. Yu, H. Jiang, X. Mu, H. Liu, *Adv. Mater.,* 2013, 25, 5075–5080.

35 S. Sun, W. Wang, L. Zhang and J. Xu, *Appl. Catal. B: Environ.*, 2012, **125**, 144.

36 Y. Guo, G. Zhang, J. Liu and Y. Zhang, *RSC Adv.*, 2013, **3**, 2963.

37 J. Bi, J. G. Che, L .Wu and M. H. Liu, *Mater. Res. Bull.*, 2013, **48**, 2071.

38 G. H. Tian, Y. J. Chen, X. Y. Meng, J. Zhou, W. Zhou, K. Pan, C. G. Tian, Z. Y. Ren and H. G. Fu, *ChemPlusChem*, 2013, **78**, 117.

39 Y. S Xu, Z. J. Zhang and W. D. Zhang, *Mater. Res. Bull.*, 2013, **48**, 1420.

40 D. Hou, W. Luo, Y. Huang, J. C. Yu and X. Hu, *Nanoscale*, 2013, **5**, 2028.

41 T. Cao, Y. Li, C. Wang, Z. Zhang, M. Zhang, C. Shao and Y. Liu, *J. Mater. Chem.*, 2011, **21**, 6922.

42 W. Wei, Y. Dai and B. Huang, *J. Phys. Chem. C*, 2009, **113**, 5658.

43 S. Li, J. Zhang, M. G. Kibria, Z. Mi, M. Chaker, D. Ma, R. Nechache and F. Rosei, *Chem. Commun.*, 2013, **49**, 5856.

44 Z. Li, Y. Shen, C. Yang, Y. Lei, Y. Guan, Y. Lin, D. Liu and C. W. Nan, *J. Mater. Chem. A*, 2013, **1**, 823.

45 Y. Huo, M. Miao, Y. Zhang, J. Zhu and H. Li, *Chem. Commun.*, 2011, **47**, 2089.

46 F. Gao, X. Y. Chen, K. B. Yin, S. Dong, Z. F. Ren, F. Yuan, T. Yu, Z. G. Zou and J. M. Liu, *Adv. Mater.,* 2007, **19**, 2889.

47 S. Li, Y. H. Lin, B. P. Zhang, Y. Wang and C. W. Nan, *J. Phys. Chem. C*, 2010, **114**, 2903.

48 Y. Zhang, A. M. Schultz, P. A. Salvadora and G. S. Rohrer, *J. Mater. Chem.*, 2011, **21**, 4168.

49 Q. Zhang , W. Gong , J. Wang , X. Ning, Z. Wang, X. Zhao, W. Ren and Z. Zhang, *J. Phys. Chem. C*, 2011, **115**, 25241.

50 S. Qi, R. Zuo, Y. Wang, H. Wong and L. W. Chan, *J. Mater. Sci.*, 2013, **48**, 4143.

51 S. Sun, W. Wang, L. Zhang and M. Shang, *J. Phys. Chem. C*, 2009, **113**, 12826.

52 Q. J. Ruan and W. D. Zhang, *J. Phys. Chem. C*, 2009, **113**, 4168.

53 S. Sun, W. Wang, H. Xu, L. Zhou , M. Shang and L. Zhang, *J. Phys. Chem. C*,

2008, **112**, 17835.

54 J. Xiong, Z. Jiao, G. Lu, W. Ren, J. Ye and Y. Bi, *Chem. Eur. J.*, 2013, **19**, 9472.

55 L. Zhang, W. Wang, S. Sun, Y. Sun, E. Gao and J. Xu, *Appl. Catal. B: Environ.*, 2013, **132–133**, 315.

56 M. Guan, C. Xiao, J. Zhang, S. Fan, R. An, Q. Cheng, J. Xie, M. Zhou, B. Ye and Y. Xie, *J. Am. Chem. Soc.*, 2013, **135**, 10411.

57 S. Sun, W. Wang, L. Zhang, L. Zhou, W. Yin and M. Shang, *Environ. Sci. Technol.*, 2009, **43**, 2005.

58 L. Zhang, W. Wang, S. Sun, Z. Zhang, J. Xu and J. Ren, *Catal. Commun.*, 2012, **26**, 88.

59 L. Zhang, H. Wang, Z. Chen, P. K. Wong and J. Liu, *Appl. Catal. B: Environ.,* 2011, 106, 1.

60 L. Zhang and Y. Zhu, *Catal. Sci. Technol.,* 2012, **2**, 694.

61 Y. Park, K. J. McDonald and K. S. Choi, *Chem. Soc. Rev.,* 2013, **42**, 2321.

62 A. R. Lim, S. H. Choh and M. S. Jang, *J. Phys: Condens. Matter*, 1995, **7**, 7309.

63 J. D. Bierlein and A. W. Sleight, *Solid State Commun.,* 1975, **16** , 69.

64 A. W. Sleight, H.-Y. Chen, A. Ferretti and D. E. Cox, *Mater. Res. Bull.,* 1979, **14**, 1571.

65 S. Tokunaga, H. Kato, and A. Kudo, *Chem. Mater.,* 2001, **13**, 4624.

66 Y. Yoneda, S. Kohara, H. Takeda and T. Tsurumi, *Jpn. J. Appl. Phys.,* 2012, **51**, 09LE06.

67 N. A. McDowell, K. S. Knight and P. Lightfoot, *Chem. Eur. J.,* 2006, **12**, 1493.

68 Z. Zhao, Z. Li and Z. Zou, *Phys. Chem. Chem. Phys.,* 2011, **13**, 4746.

69 A. Walsh, Y. Yan, M. N. Huda, M. M. Al-Jassim and S. H. Wei, *Chem. Mater.*, 2009, **21**, 547.

70 K. Lai, W. Wei, Y. Dai, R. Zhang and B. Huang, *Rare Metals*, 2011, **30**, 166.

71 H. Fu, C. Pan, W. Yao and Y. Zhu, J. Phys. Chem. B, 2005, 109, 22432-22439

72 M. Oshikiri and M. Boero, *J. Phys. Chem. B,* 2006, **110**, 9188.

73 Y. Xu and M. A. A. Schoonen, *Am. Mineral.,* 2000, **85**, 543.

74 M. Long, W. Cai, J. Cai, B. Zhou, X. Chai and Y. Wu, *J. Phys. Chem. B,* 2006, **110**, 20211.

75 R. G. Pearson, *Inorg. Chem.,* 1988, **27**, 734.

76 N. Umezawa, O. Shuxin and J. H. Ye, *Phys. Rev. B*, 2011, **83**, 035202.

77 K. Lai, W. Wei, Y. Zhu, M. Guo, Y. Dai and B. Huang, *J. Solid State Chem.,* 2012, **187**, 103.

78 A. Hagfeldt and M. Gratzel, *Chem. Rev.,* 1995, **95**, 49.

79 L. Zhou, W. Wang, S. Liu, L. Zhang, H. Xu and W. Zhu, *J. Mol. Catal. A: Chem.,* 2006, **252**, 120.

80 S. Zhang, C. Zhang, Y. Man and Y. Zhu, *J. Solid State Chem.,* 2006, **179**, 62.

81 J. Yu and A. Kudo, *Chem. Lett.,* 2005, **34**, 1528.

82 M. Shang, W. Wang, S. Sun, L. Zhou and L. Zhang, *J. Phys. Chem. C,* 2008, **112**, 10407.

83 S. Obregón, A. Caballero and G. Colón, *Appl. Catal. B: Environ.,* 2012, **117–118**, 59.

84 L. Ren, L. Ma, L. Jin, J. B. Wang, M. Qiu and Y. Yu, *Nanotechnology,* 2009, **20**, 405602.

85 C. Zhang and Y. Zhu, *Chem. Mater,* 2005, **17**, 3537.

86 H. Fu, L. Zhang, W. Yao and Y. Zhu, *Appl. Catal. B: Environ.,* 2006, **66**, 100.

87 Y. Zhao, Y. Xie, X. Zhu, S. Yan and S. Wang, *Chem. Eur. J.,* 2008, **14**, 1601.

88 L. Zhou, W. Wang and H. Xu, *Cryst. Growth Des.,* 2008, **8**, 728.

89 W. Yin, W. Wang, M. Shang, L. Zhang and J. Ren, *Chem. Lett.,* 2009, **38**, 422.

90 L. Zhou, W. Wang, L. Zhang, H. Xu and W. Zhu, *J. Phys. Chem. C,* 2007, **111**, 13659.

91 Y. Sun, C. Wu, R. Long, Y. Cui, S. Zhang and Y. Xie, *Chem. Commun.,* 2009, 4542.

92 M. Shang, W. Wang, S. Sun, J. Ren, L. Zhou and L. Zhang, *J. Phys. Chem. C,* 2009, **113**, 20228.

93 H. Jiang, H. Dai, X. Meng, K. Ji, L. Zhang and J. Deng, *Appl. Catal. B: Environ.,* 2011, **105**, 326.

94 J. W. Tang, Z. G. Zou and J. H. Ye, *Catal. Lett.,* 2004, **92**, 53.

95 L. Zhang, W. Wang, Z. Chen, L. Zhou, H. Xu and W. Zhu, *J. Mater. Chem.,* 2007, **17**, 2526.

96 Z. Q. Li, X. T. Chen and Z. L. Xue, *CrystEngComm,* 2013, **15**, 498.

97 J. Wu, F. Duan, Y. Zheng and Y. Xie, *J. Phys. Chem. C,* 2007, **111**, 12866.

98 Z. Chen, L. Qian, J. Zhu, Y. Yuan and X. Qian, *CrystEngComm,* 2010, **12**, 2100.

99 F. Amano, K. Nogami, R. Abe and B. Ohtani, *J. Phys. Chem. C,* 2008, **112**, 9320.

100 D. Ma, S. Huang, W. Chen, S. Hu, F. Shi and K. Fan, *J. Phys. Chem. C,* 2009, **113**, 4369.

101 D. He, L. Wang, H. Li, T. Yan, D. Wang and T. Xie, *CrystEngComm,* 2011, **13**, 4053.

102 L. Xu, X. Yang, Z. Zhai and W. Hou, *CrystEngComm,* 2011, **13**, 7267.

103 H. Huang, H. Chen, Y. Xia, X. Tao, Y. Gan, X. Weng and W. Zhang, *J. Colloid Interface Sci.,* 2012, **370**, 132.

104 S. Liu and J. Yu, *J. Solid State Chem.,* 2008, **181**, 1048.

105 Z. Cui, D. Zeng, T. Tang, J. Liu and C. Xie, *J. Hazard. Mater.,* 2010, **183**, 211.

106 G. Li, D. Zhang, J. C. Yu and M. K. H. Leung, *Environ. Sci. Technol.,* 2010, **44**, 4276.

107 G. Tian, Y. Chen, W. Zhou, K. Pan, Y. Dong, C. Tian and H. Fu, *J. Mater. Chem.,* 2011, **21**, 887.

108 F. Amano, K. Nogami and B. Ohtani, *J. Phys. Chem. C,* 2009, **113**, 1536.

109 G. Li, D. Zhang and J. C. Yu, *Chem. Mater.,* 2008, **20**, 3983.

110 L. W. Zhang, Y. J. Wang, H. Y. Cheng, W. Q. Yao and Y. F. Zhu, *Adv. Mater.,* 2009, **21**, 1286.

111 S. Sun, W. Wang and L. Zhang, *J. Mater. Chem.,* 2012, **22**, 19244.

112 S. Sun, W. Wang, L. Zhou and H. Xu, *Ind. Eng. Chem. Res.,* 2009, **48**, 1735.

113 L. Zhang, D. Chen and X. Jiao, *J. Phys. Chem. B,* 2006, **110**, 2668.

114 D. Wang, H. Jiang, X. Zong, Q. Xu, Y. Ma, G. Li and C. Li, *Chem.-Eur. J.,* 2011, **17**, 1275.

115 Z. Zhao, Z. Li and Z. Zou, *RSC Advances,* 2011, **1**, 874.

116 G. Xi and J. Ye, *Chem. Commun.,* 2010, **46**, 1893.

117 A. K. P. Mann, E. M. P. Steinmiller and S. E. Skrabalak, *Dalton Trans.,* 2012, **41**, 7939.

118 T. Saison, N. Chemin, C. Chanéac, O. Durupthy, V. Ruaux, L. Mariey, F. Maugé, P. Beaunier and J. P. Jolivet, *J. Phys. Chem. C,* 2011, **115**, 5657.

119 H. Fu, S. Zhang, T. Xu, Y. Zhu and J. Chen, *Environ. Sci. Technol.*, 2008, **42**, 2085.

120 S. Liu, K. Yin, W. Ren, B. Cheng and J. Yu, *J. Mater. Chem.,* 2012, **22**, 17759.

121 W. Luo, Z. Li, T. Yu and Z. Zou, *J. Phys. Chem. C,* 2012, **116**, 5076.

122 W. Yao, H. Iwai and J. Ye, *Dalton Trans.,* 2008, 1426.

123 W. Luo, Z. Yang, Z. Li, J. Zhang, J. Liu, Z. Zhao, Z. Wang, S. Yan, T. Yu and Z.

Zou, *Energy Environ. Sci.,* 2011, **4**, 4046.

124 H. Ye, J. Lee, J. S. Jang and A. J. Bard, *J. Phys. Chem. C,* 2010, **114**, 13322.

125 H. S. Park, K. E. Kweon, H. Ye, E. Paek, G. S. Hwang and A. J. Bard, *J. Phys. Chem. C,* 2011, **115**, 17870.

126 S. P. Berglund, A. J. E. Rettie, S. Hoang and C. B. Mullins, *Phys. Chem. Chem. Phys.,* 2012, **14**, 7065.

127 W. Luo, J. Wang, X. Zhao, Z. Zhao, Z. Li and Z. Zou, *Phys. Chem. Chem. Phys.,* 2013, **15**, 1006.

128 L. Zhou, M. Yu, J. Yang, Y. Wang and C. Yu, *J. Phys. Chem. C,* 2010, **114**, 18812.

129 L. Zhang, Y. Man and Y. Zhu, *ACS Catal.,* 2011, **1**, 841.

130 X. C. Song, Y. F. Zheng, R. Ma, Y. Y. Zhang and H. Y. Yin, *J. Hazard. Mater.,* 2011, **192**, 186.

131 H. Yu, Z. Zhu, J. Zhou, J. Wang, J. Li and Y. Zhang, *Appl. Surf. Sci.,* 2013, **265**, 424.

132 Z. Zhang, W. Wang, E. Gao, M. Shang and J. Xu, *J. Hazard. Mater.,* 2011, **196**, 255.

133 R. Shi, G. Huang, J. Lin and Y. Zhu, *J. Phys. Chem. C,* 2009, **113**, 19633.

134 M. Shang, W. Z. Wang, L. Zhang and H. L. Xu, *Mater. Chem. Phys.,* 2010, **120**, 155.

135 M. Long, W. Cai and H. Kisch, *J. Phys. Chem. C,* 2008, **112**, 548.

136 H. Jiang, M. Nagai and K. Kobayashi, *J. Alloys Compd.,* 2009, **479**, 821.

137 J. Su, X. X. Zou, G. D. Li, X. Wei, C. Yan, Y. N. Wang, J. Zhao, L. J. Zhou and J. S. Chen, *J. Phys. Chem. C,* 2011, **115**, 8064.

138 N. Wetchakun, S. Chaiwichain, B. Inceesungvorn, K. Pingmuang, S.

Phanichphant, A. I. Minett and J. Chen, *ACS Appl. Mater. Inter.,* 2012, **4**, 3718.

139 L. Chen, Q. Zhang, R. Huang, S. F. Yin, S. L. Luo and C. T. Au, *Dalton Trans.,* 2012, **41**, 9513.

140 M. L. Guan, D. K. Ma, S. W. Hu, Y. J. Chen and S. M. Huang, *Inorg. Chem.,* 2011, **50**, 800.

141 D. K. Ma, M. L. Guan, S. S. Liu, Y. Q. Zhang, C. W. Zhang, Y. X. He and S. M. Huang, *Dalton Trans.,* 2012, **41**, 5581.

142 W. Zhao, Y. Wang, Y. Yang, J. Tang and Y. Yang, *Appl. Catal. B: Environ.,* 2012, **115–116**, 90.

143 W. Wang, X. Huang, S. Wu, Y. Zhou, L. Wang, H. Shi, Y. Liang and B. Zou, *Appl. Catal. B: Environ.,* 2013, **134-135**, 293.

144 J. Su, L. Guo, N. Bao and C. A. Grimes, *Nano Lett.,* 2011, **11**, 1928.

145 S. J. Hong, S. Lee, J. S. Jang and J. S. Lee, *Energy Environ. Sci.,* 2011, **4**, 1781.

146 P. Chatchai, Y. Murakami, S. Kishioka, A. Y. Nosaka and Y. Nosaka, *Electrochimica Acta,* 2009, **54**, 1147.

147 R. Saito, Y. Miseki and K. Sayama, *Chem. Commun.,* 2012, **48**, 3833.

148 Y. Liang, T. Tsubota, L. P. A. Mooij and R. van de Krol, *J. Phys. Chem. C,* 2011, **115**, 17594.

149 M. Shang, W. Wang, L. Zhang, S. Sun, L. Wang and L. Zhou, *J. Phys. Chem. C,* 2009, **113**, 14727.

150 S. Murcia-López, M. C. Hidalgo and J. A. Navío, *Appl. Catal. A: Gen.,* 2012, **423–424**, 34.

151 S. M. López, M. C. Hidalgo and J. A. Navío, G. Colón, *J. Hazard. Mater.,* 2011, **185**, 1425.

152 J. Xu, W. Wang, S. Sun and L. Wang, *Appl. Catal. B: Environ.,* 2012, **111-112**,

126.

153 Y. Zheng, K. Lv, X. Li, K. Deng, J. Sun, L. Chen, L. Cui and D. Du, *Chem. Eng. Technol.,* 2011, **34**, 1630.

154 Y. Zhou, F. Krumeich, A. Heel and G. R. Patzke, *Dalton Trans.,* 2010, **39**, 6043.

155 G. Colón, S. M. López, M. C. Hidalgo and J. A. Navío, *Chem. Commun.,* 2010, **46**, 4809.

156 Q. C. Xu, Y. H. Ng, Y. Zhang, J. S. C. Loo, R. Amal and T. T. Y. Tan, *Chem. Commun.,* 2011, **47**, 8641.

157 Y. Zhang, L. Fei, X. Jiang, C. Pan and Y. Wang, *J. Am. Ceram. Soc.,* 2011, **94**, 4157.

158 Q. C. Xu, D. V. Wellia, Y. H. Ng, R. Amal and T. T. Y. Tan, *J. Phys. Chem. C,* 2011, **115**, 7419.

159 M. S. Gui and W. D. Zhang, *Nanotechnology,* 2011, **22**, 265601.

160 M. Ge, Y. Li, L. Liu, Z. Zhou and W. Chen, *J. Phys. Chem. C,* 2011, **115**, 5220.

161 X. Li, R. Huang, Y. Hu, Y. Chen, W. Liu, R. Yuan and Z. Li, *Inorg. Chem.,* 2012, **51**, 6245.

162 M. S. Gui, W. D. Zhang, Q. X. Su and C. H. Chen, *J. Solid State Chem.,* 2011, **184**, 1977.

163 Y. Wang, X. Bai, C. Pan, J. He and Y. Zhu, *J. Mater. Chem.,* 2012, **22**, 11568.

164 L. Ge, C. Han and J. Liu, *Appl. Catal. B: Environ.,* 2011, **108-109**, 100.

165 M. S. Gui, W. D. Zhang, Y. Q. Chang and Y. X. Yu, *Chem. Engin. J.,* 2012, **197**, 283.

166 Q. Xiao, J. Zhang, C. Xiao and X. Tan, *Catal. Commun.,* 2008, **9**, 1247.

167 L. Ge and J. Liu, *Appl. Catal. B: Environ.,* 2011, **105**, 289.

168 Y. L. Min, K. Zhang, Y. C. Chen, Y. G. Zhang and W. Zhao, *Sep. Purif.*

Technol., 2012, **92**, 115.

169 D. He, L. Wang, D. Xu, J. Zhai, D. Wang and T. Xie, *ACS Appl. Mater. Inter.,* 2011, **3**, 3167.

170 Z. Zhang, W. Wang, L. Wang and S. Sun, *ACS Appl. Mater. Inter.,* 2012, **4**, 593.

171 Y. Sun, B. Qu, Q. Liu, S. Gao, Z. Yan, W. Yan, B. Pan, S. Wei and Y. Xie, *Nanoscale,* 2012, **4**, 3761.

172 Y. H. Ng, A. Iwase, A. Kudo and R. Amal, *J. Phys. Chem. Lett.,* 2010, **1**, 2607.

173 Y. Zhang, J. Yu, H. Wang, M. Sun, Y. Bu, D. Yu and W. Li, *J. Nanotechnol.,* 2011, **2011**, 702130.

174 S. Sun, W. Wang and L. Zhang, *J. Phys. Chem. C,* 2013, **117**, 9113.

175 E. Gao, W. Wang, M. Shang and J. Xu, *Phys. Chem. Chem. Phys.,* 2011, **13**, 2887.

176 Y. L. Min, K. Zhang, Y. C. Chen and Y. G. Zhang, *Sep. Purif. Technol.,* 2012, **86**, 98.

177 H. Ma, J. Shen, M. Shi, X. Lu, Z. Li, Y. Long, N. Li and M. Ye, *Appl. Catal. B: Environ.,* 2012, **121-122**, 198.

178 F. Zhou, R. Shi and Y. Zhu, *J. Mol. Catal. A: Chem.,* 2011, **340**, 77.

179 P. Wang, Y. Ao, C. Wang, J. Hou and J. Qian, *Carbon,* 2012, **50**, 5256.

180 S. Zhu, T. Xu, H. Fu, J. Zhao and Y. Zhu, *Environ. Sci. Technol.,* 2007, **41**, 6234.

181 Y. Li, J. Liu, X. Huang and J. Yu, *Dalton Trans.,* 2010, **39**, 3420.

182 Y. Chen, X. Cao, J. Kuang, Z. Chen, J. Chen and B. Lin, *Catal. Commun.,* 2010, **12**, 247.

183 M. Zhang, C. Shao, J. Mu, X. Huang, Z. Zhang, Z. Guo, P. Zhang and Y. Liu, *J. Mater. Chem.,* 2012, **22**, 577.

184 X. Zhao, H. Liu, Y. Shen and J. Qu, *Appl. Catal. B: Environ.,* 2011, **106**, 63.

185 D. Tang, H. Zhang, H. Huang, R. Liu, Y. Han, Y. Liu, C. Tong and Z. Kang, *Dalton Trans.,* 2013, **42**, 6285.

186 S. W. Cao, Z. Yin, J. Barber, F. Y. C. Boey, S. C. J. Loo and C. Xue, *ACS Appl. Mater. Inter.,* 2012, **4**, 418.

187 J. Ren, W. Wang, S. Sun, L. Zhang and J. Chang, *Appl. Catal. B: Environ.,* 2009, **92**, 50.

188 D. Wang, G. Xue, Y. Zhen, F. Fu and D. Li, *J. Mater. Chem.,* 2012, **22**, 4751.

189 L. Ge, *J. Mol. Catal. A: Chem.,* 2008, **282**, 62.

190 L. Ge, *Mater. Chem. Phys.,* 2008, **107**, 465.

191 S. Kohtani, J. Hiro, N. Yamamoto, A. Kudo, K. Tokumura and R. Nakagaki, *Catal. Commun.,* 2005, **6**, 185.

192 S. Kohtani, M. Tomohiro, K. Tokumura and R. Nakagaki, *Appl. Catal. B: Environ.,* 2005, **58**, 265.

193 J. W. Tang, J. R. Durrant and D. R. Klug, *J. Am. Chem. Soc.,* 2008, **130**, 13885.

194 K. Sayama, A. Nomura, T. Arai, T. Sugita, R. Abe, M. Yanagida, T. Oi, Y. Iwasaki, Y. Abe and H. Sugihara, *J. Phys. Chem. B,* 2006, **110**, 11352.

195 J. A. Seabold and K. S. Choi, *J. Am. Chem. Soc.,* 2012, **134**, 2186.

196 D. K. Zhong, S. Choi and D. R. Gamelin, *J. Am. Chem. Soc.,* 2011, **133**, 18370.

197 S. K. Pilli, T. E. Furtak, L. D. Brown, T. G. Deutsch, J. A. Turner and A. M. Herring, *Energy Environ. Sci.,* 2011, **4**, 5028.

198 F. F. Abdi and R. van de Krol, *J. Phys. Chem. C,* 2012, **116**, 9398.

199 D. Wang, R. Li, J. Zhu, J. Shi, J. Han, X. Zong and C. Li, *J. Phys. Chem. C,* 2012, **116**, 5082.

200 T. H. Jeon, W. Choi and H. Park, *Phys. Chem. Chem. Phys.,* 2011, **13**, 21392.

201 S. K. Pilli, T. G. Deutsch, T. E. Furtak, J. A. Turner, L. D. Brown and A. M.

Herring, *Phys. Chem. Chem. Phys.,* 2012, **14**, 7032.

202 M. Zhou, J. Bao, W. Bi, Y. Zeng, R. Zhu, M. Tao and Y. Xie, *ChemSusChem,* 2012, **5**, 1420.

203 M. W. Kanan and D. G. Nocera, *Science,* 2008, **321**, 1072.

204 J. G. McAlpin, Y. Surendranath, M. Dinca, T. A. Stich, S. A. Stoian, W. H. Casey, D. G. Nocera and R. D. Britt, *J. Am. Chem. Soc.,* 2010, **132**, 6882.

205 F. Lin, D. Wang, Z. Jiang, Y. Ma, J. Li, R. Li and C. Li, *Energy Environ. Sci.,* 2012, **5**, 6400.

206 J. Xu, W. Wang, E. Gao, J. Ren and L. Wang, *Catal. Commun.,* 2011, **12**, 834.

Figure captions

Fig. 1 Schematic crystal structure of $BiVO_4$, Bi_2WO_6 and Bi_2MoO_6 in the polyhedron mode: (a) Scheelite $BiVO_4$, (b) Aurivillius orthorhombic Bi_2WO_6, (c) Aurivillius orthorhombic Bi_2MoO_6.

Fig. 2 Schematic band structure and the calculated redox potentials of $BiVO_4$, Bi_2WO_6 and Bi_2MoO_6 at the point of zero charge.

Fig. 3 (a) Representative TEM image of dendrite $BiVO_4$ from ref. 87. (b) Representative TEM and SEM image of flower-like $BiVO_4$ from ref. 90. (c) Representative SEM image of olive-like $BiVO_4$ from ref. 91. Reprinted with permission. Copyright 2008, 2007 and 2009, Wiley-VCH, American Chemical Society and Royal Society of Chemistry.

Fig. 4 Typical SEM images of flower-like Bi_2WO_6 hierarchical structures from ref. 95. Reprinted with permission. Copyright 2007, Royal Society of Chemistry.

Fig. 5 (a) TEM image of ordered mesoporous $BiVO_4$ using KIT-6 as a template from ref. 109. (b) SEM image of ordered macroporous Bi_2WO_6 film synthesized with 340 nm carbon spheres from ref. 110. (c) TEM image of three-dimensional ordered macroporous Bi_2WO_6 powder synthesized with 90 nm SiO_2 spheres from ref. 111. Reprinted with permission. Copyright 2008, 2009 and 2012, American Chemical Society, Wiley-VCH and Royal Society of Chemistry.

Fig. 6 (a) TEM image of {010} oriented $BiVO_4$ nanoplates from ref. 112. (b) TEM image of {010} oriented $BiVO_4$ nanosheets from ref. 113. (c) Schematic illustration of monoclinic $BiVO_4$ crystal structure viewed along different directions (1×1×1 cell) to show the structural feature of the (101), (100), (001) and (010) facets from ref. 112. Reprinted with permission. Copyright 2009 and 2006, American Chemical Society.

Fig. 7 UV -visible spectral changes of RhB (2×10^{-5} M, 50 mL) over Bi_2WO_6 and fluorinated Bi_2WO_6 photocatalyst from ref. 119. Reprinted with permission. Copyright 2008, American Chemical Society.

Fig. 8 Possible sketch of the transfer of photogenerated electrons in Mo-doped $BiVO_4$ electrodes illuminated from the front side and the back side before and after the electrochemical pretreatment. (Reproduced from ref. 121 with permission from American Chemistry Society)

Fig. 9 Mott–Schottky plots for pure $BiVO_4$ and Mo-doped $BiVO_4$ in 0.5 M Na_2SO_4, the ac amplitude is 10 mV and the frequency is 1000 Hz. (Reproduced from ref. 123 with permission from The Royal Society of Chemistry)

Fig. 10 The total and partial DOS of relaxed Bi_2WO_6: (a) with one O vacancy, (b) with one N atom, (c) with two N atoms. The navy dashed line represents the Fermi level from ref. 77. Reprinted with permission. Copyright 2012, Elsevier.

Fig. 11 (a) Transient photovoltage (TPV) responses of bare $BiVO_4$, bare V_2O_5, and 5.3 wt % V_2O_5-$BiVO_4$, (b) Schematic diagram for electron hole separation at the interface of the V_2O_5-$BiVO_4$ material from ref. 137. Reprinted with permission. Copyright 2011, American Chemistry Society.

Fig. 12 (a) The schematic diagram illustrates the recombination at the defect state present at the FTO/$BiVO_4$ interface and the hole mirror effect of the SnO_2 layer, (b) Comparison of the IPCE spectra of $BiVO_4$ on FTO with and without an ~ 10 nm SnO_2 interfacial layer. (Reproduced from ref. 148 with permission from American Chemistry Society)

Fig. 13 (a) TEM image of the RGO-Bi_2WO_6 QDs, (b) The schematic illustration of charge carrier transfer in RGO-Bi_2WO_6 QDs. (Reproduced from ref. 174 with

permission from American Chemistry Society)

Fig. 14 Schematic illustration of the detailed energy alignment in the Au-$BiVO_4$ heterogeneous structure and the proposed mechanism of photocatalytic water oxidation by Au-$BiVO_4$ nanosheets in the presence of sacrificial agent $S_2O_8^{2-}$. The Fermi level (E_f) of Au shifts to mo re negative potentials (E_f^*) because of the transfer of photogenerated electrons from $BiVO_4$ to Au. The SPR excitation of the gold nanoparticle is believed to enhance electron−hole separation near the Au-$BiVO_4$ heterojunction. (Ref. 186 with permission from American Chemistry Society)

Fig. 15 Energy diagram showing the kinetic processes active in the Co-Pi/W:$BiVO_4$ PEC photoanodes. Electron-hole pairs are generated with a current density associated with photon-absorption (J_{abs}) and can recombine nonproductively with current densities associated with radiative or nonradiative bulk (J_{br}) and surface (J_{sr}) recombination. Electron collection at the back contact (J_{PEC}) and hole transfer to the oxidizable substrate (J_{ox}) are productive processes contributing to PEC device efficiency. (Ref. 196 with permission from American Chemistry Society)

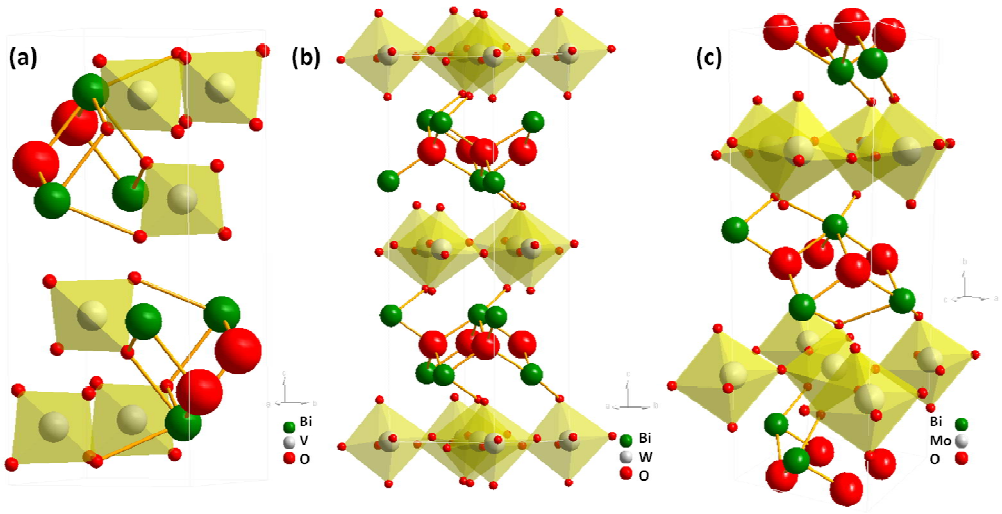

Fig. 1

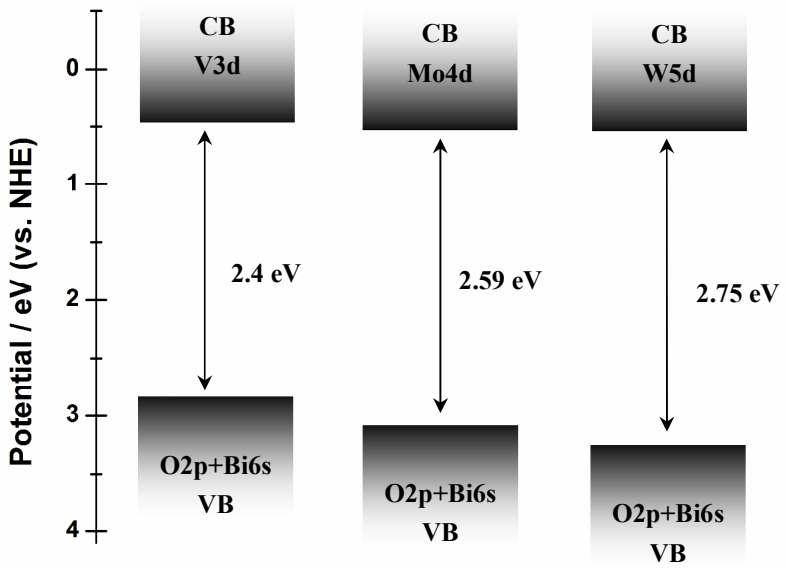

Fig. 2

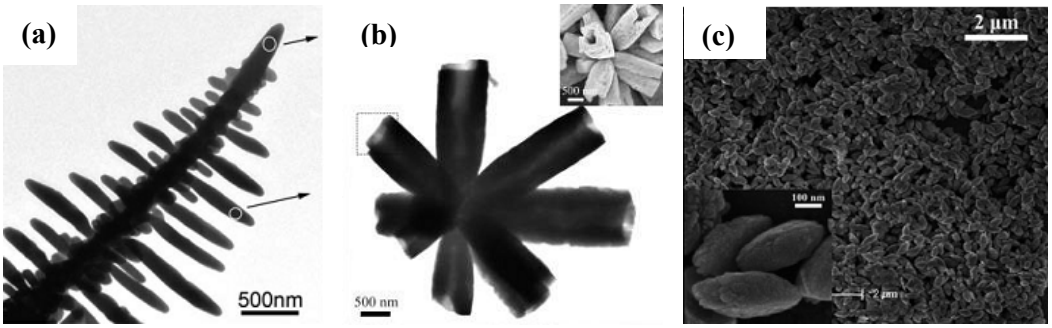

Fig. 3

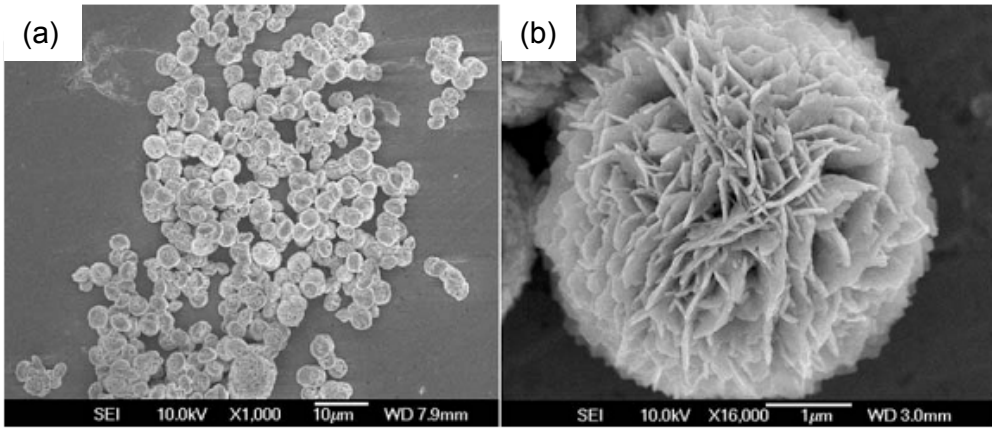

Fig. 4

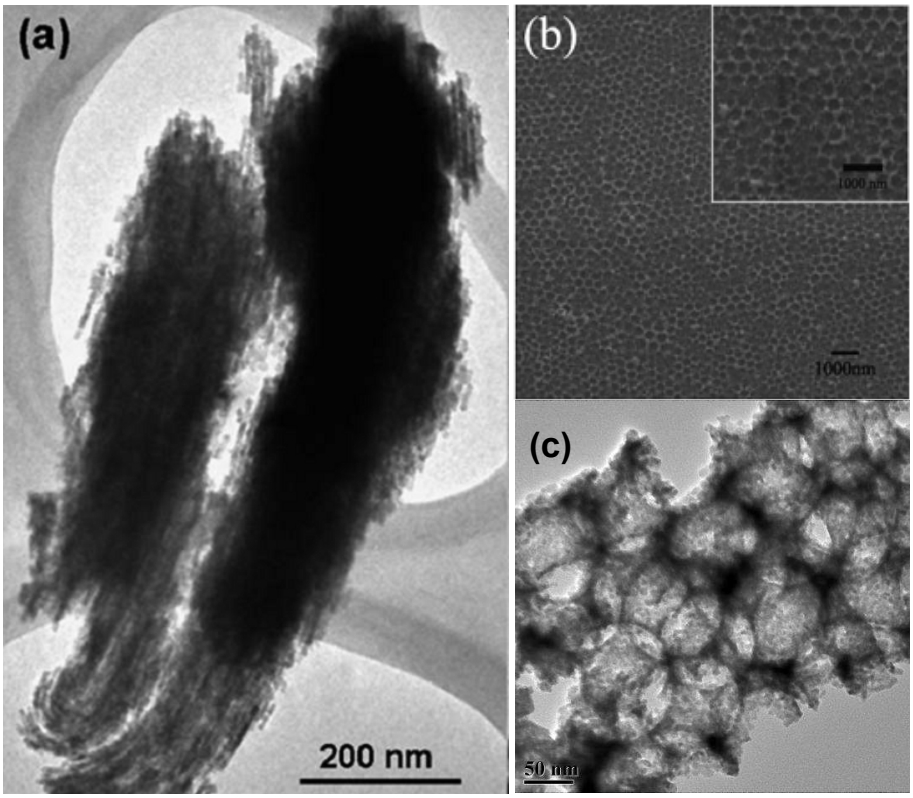

Fig. 5

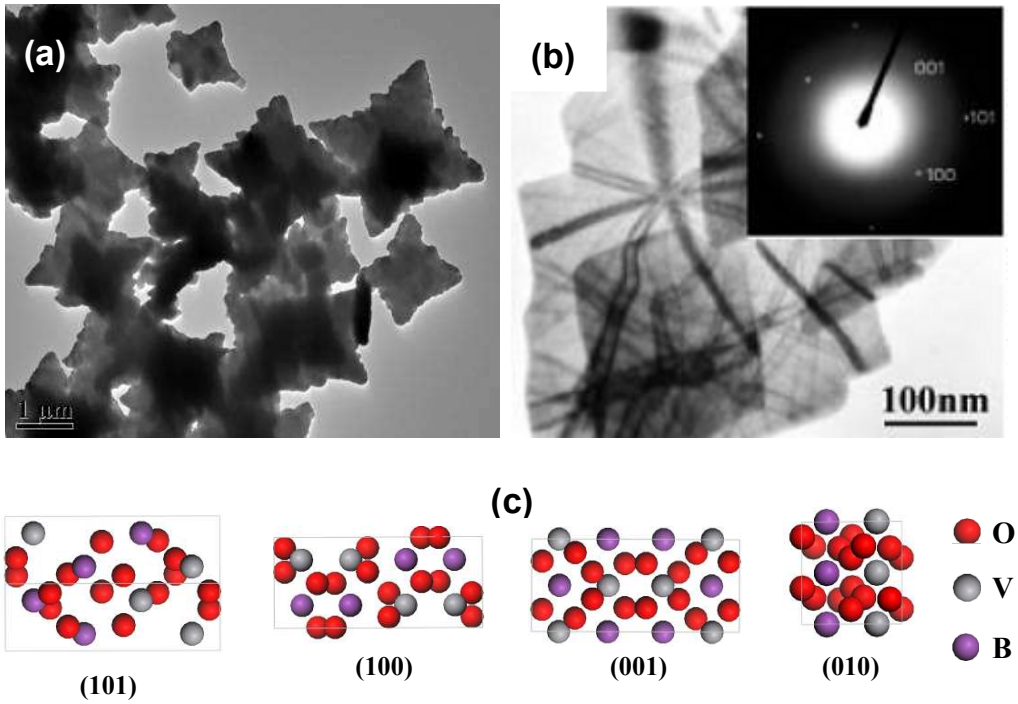

Fig. 6

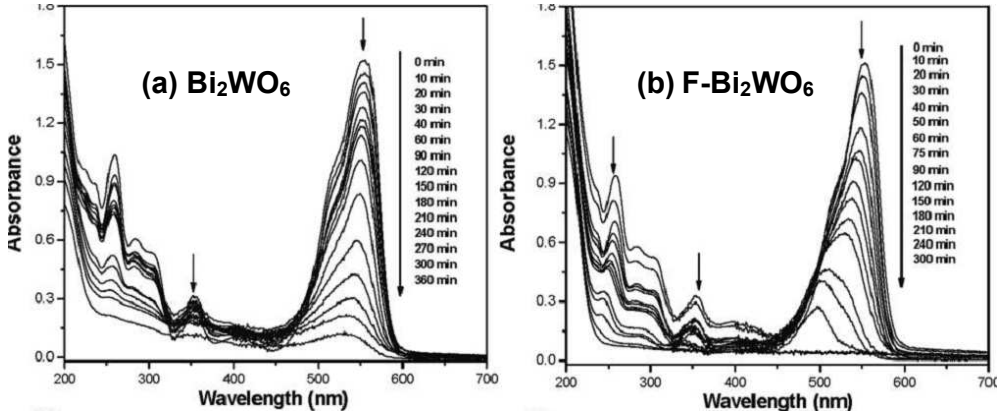

Fig. 7

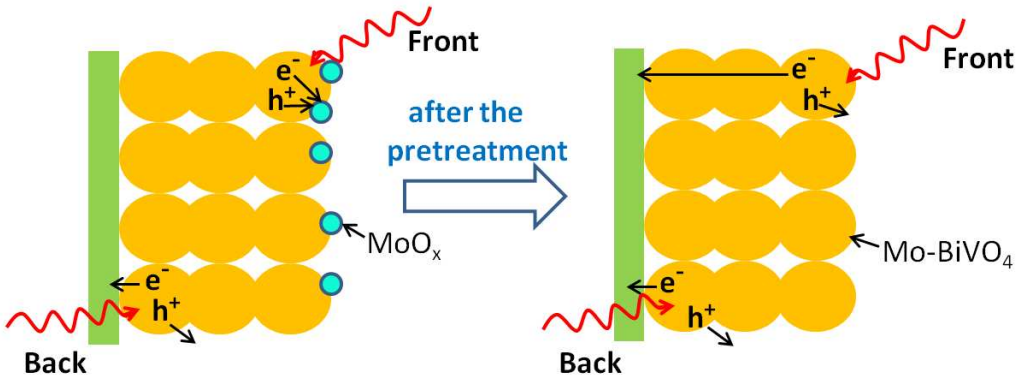

Fig. 8

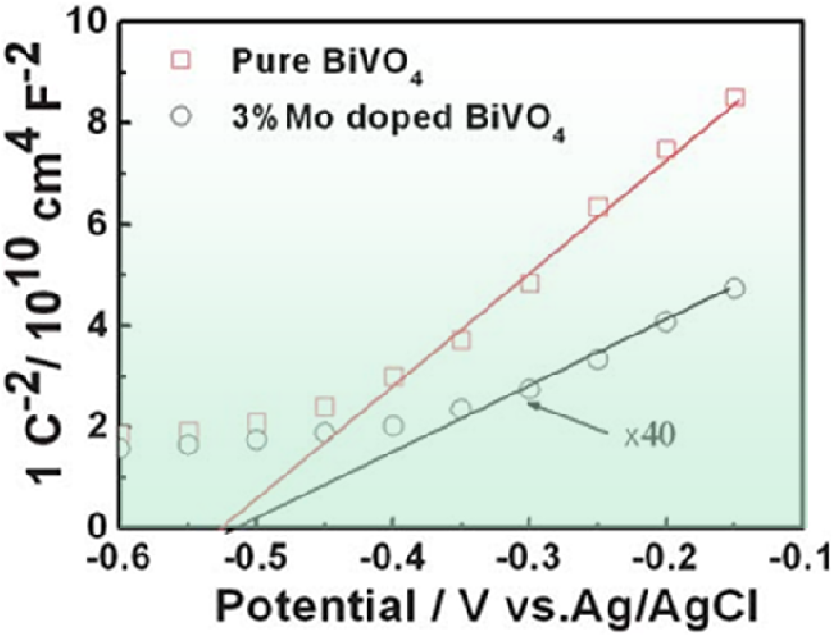

Fig. 9

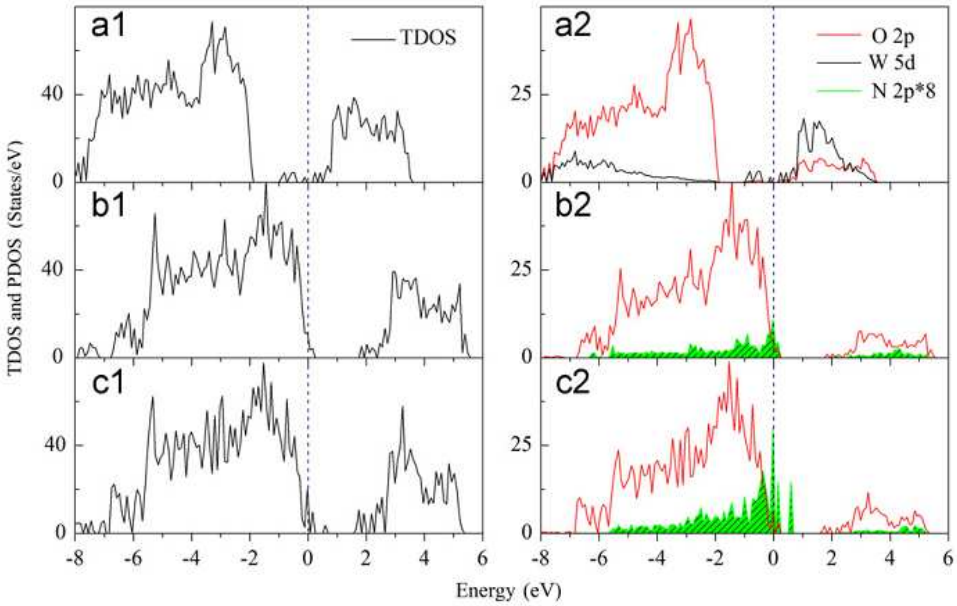

Fig. 10

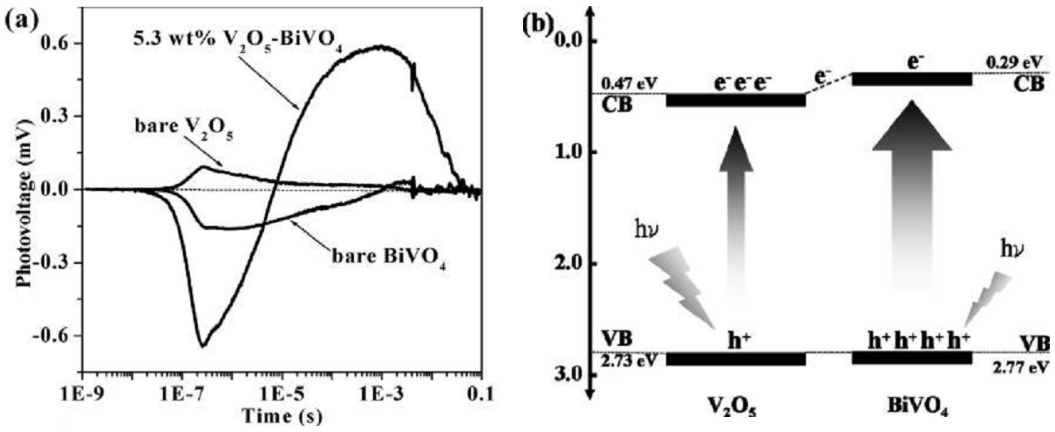

Fig. 11

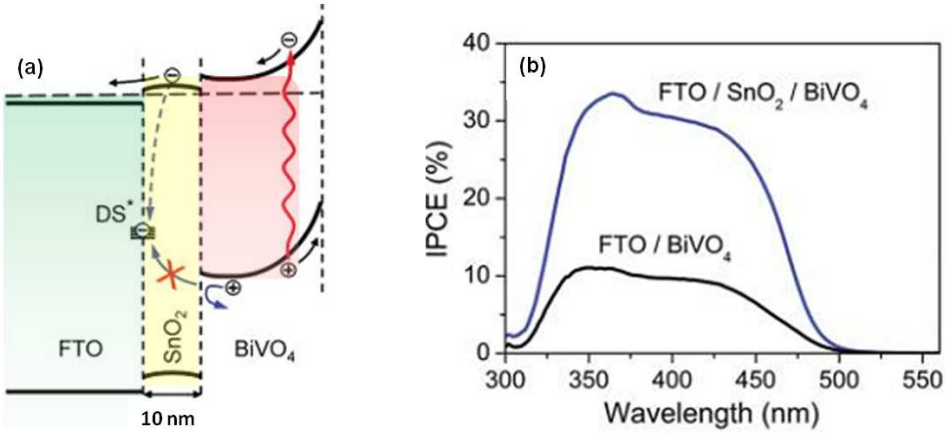

Fig. 12

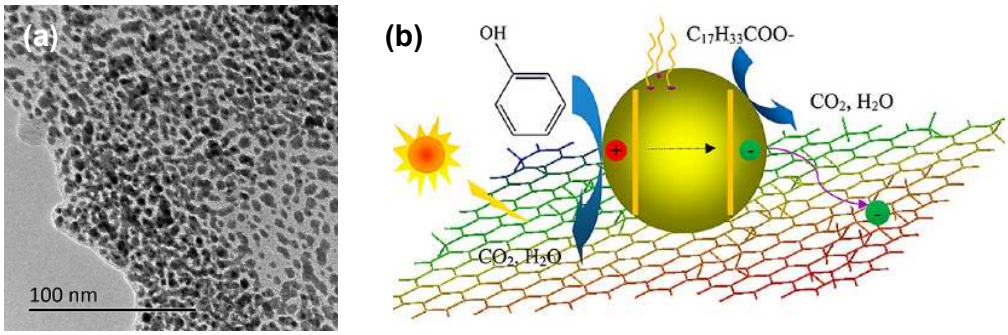

Fig. 13

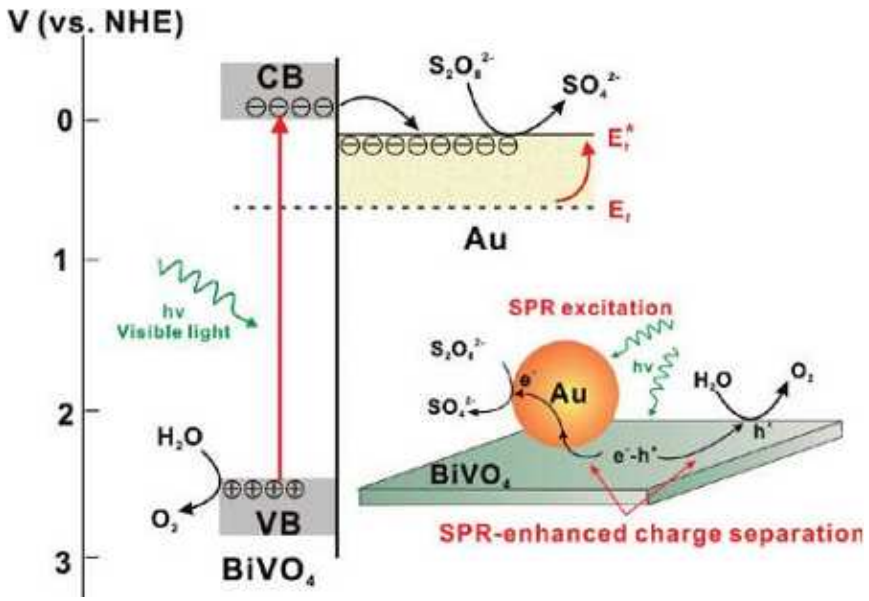

Fig. 14

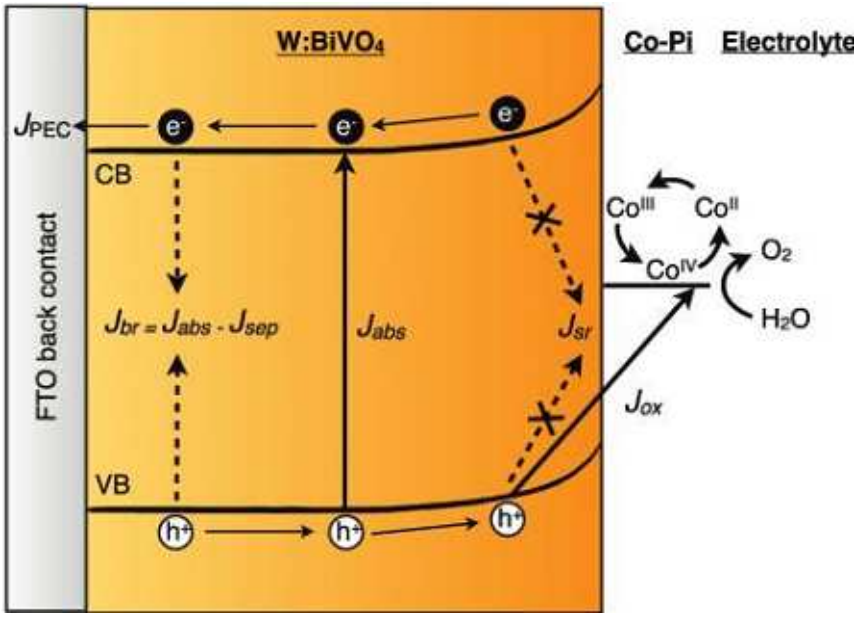

Fig. 15

Bismuth based complex oxide photocatalysts with high activity and stability could be obtained by engineering chemical compositions, morphologies, and microstructures.